An Najah National University
Faculty of Graduate Studies

Flux Simulation and Studies of the First X-Ray Beam of the ThomX Project

By
Hend Saleem Shahed

Supervisor
Prof. Ghassan Saffarini

Co-Supervisor
Dr. Ahmed Bassalat

This Thesis is Submitted in Partial Fulfillment of the Requirements for the Degree of Master of Physics, Faculty of Graduate Studies, An-Najah National University, Nablus, Palestine.

2018

Flux Simulation and Studies of the First X-Ray Beam of the ThomX Project

By

Hend Saleem Shahed

This Thesis was Defended Successfully on 25/ 9/ 2018 and approved by:

Defense Committee Members		**Signature**
1. Prof. Ghassan Saffarini	/ Supervisor	…………
2. Dr. Ahmed Bassalat	/ Co-Supervisor	…………
3. Dr. Muayad Abu Saa	/ External Examiner	…………
4. Dr. Mohammed Abu-Jafar	/ Internal Examiner	…………

Dedication

This thesis is dedicated to my father, who taught me that the best kind of knowledge to have is the one which is learned for its own purpose. It is also dedicated to my mother, who taught me that even the largest task can be accomplished if it is done one step at a time.

To my dear husband, Mutaz who remains willing to engage with the struggle, and ensuing discomfort. Very special thanks for his practical and emotional support as he always supports and helps me to deal with the competing demands of studying and personal development.

Acknowledgement

I would like to express my deepest gratitude to my thesis supervisor Professor Ghassan Saffarini for his support, collegiality, assistance, information and his valuable input, to the writing process until the completion of this thesis. Without his guidance and constant feedback this research would not have been achievable.

Special thanks to Dr. Ahmed Bassalat for his time and effort, also for offer- ing me this internship opportunity in France.

I would thank Dr. Muayad Abu Saa and Dr. Mohammed Abu-Jafar for their time and acceptance to be in my defense committee.

I gratefully acknowledge the six months internship funding received towards my research from the Linear Accelerator laboratory (LAL), Orsay, France.

I greatly appreciate the support received through the collaborative work undertaken with Marie Jacquet LAL Department of Accelerators (Depacc).

I am very honored to be the recipient of this internship.

I would like to extend my thanks to those who offered collegial guidance and support: all my Professors at An-Najah National University and the Depacc team.

الإقرار

أنا الموقعة أدناه مقدمة الرسالة التي تحمل عنوان:

محاكاة ودراسة تدفق أول شعاع سيني من مشروع تومكس

Flux Simulation and Studies of the First X-ray Beam of ThomX Project

أقر بأن ما شملت عليه هذه الرسالة، إنما هي نتاج جهدي الخاص ، بإستثناء ما تمت الإشارة إليه حيثما ورد ، وأن هذه الرسالة ككل أو أي جزء منها لم يقدم من قبل لنيل أي درجة علمية أو بحث علمي أو بحثي لدى أي مؤسسة تعليمية أو بحثية أخرى.

Declaration

The work provided in this thesis unless otherwise referenced, is the researcher's own work, and has not been submitted elsewhere for any other degree or qualification.

Student's Name:	هند سليم شاهد	اسم الطالب:
Signature:	........................هند......	التوقيع:
Date:	25/9/2018	التاريخ:

Table of Contents

List of Figures

List of Tables

Flux Simulation and Studies of the First X-Ray Beam of ThomX Project

By
Hend Saleem Shahed
Supervisor
Prof. Dr. Ghassan Saffarini
Co-supervisor
Dr. Ahmed Bassalat

Abstract

In the present work, the angular and spectral flux of the Compton backscattering X-ray source of ThomX are investigated. ThomX is a shortened form of Thomson scattering producing hard X-rays.

This work was performed through two steps. Firstly, a short computer pro- gram is written by using analytical formulas allowing the calculation of the expected angular and spectral flux of the Compton source as a function of the characteristics of the incoming electron beam. Then, the CAIN program is used to generate Compton photons in order to describe X-ray spectral and angular distributions and check the agreement between the analytical formulas and CAIN simulations.

The CdTe detector parameters (the detector size and distance to the end- station), which will be used in ThomX, were also taken into consideration in the calculations. One important feature is that this simulation code can be run by accessing a giant server computer station in LAL.

The best electron parameters in ThomX are investigated to allow producing the highest Compton flux in a given energy bandwidth and a given angular aperture. The effect on the Compton flux of both the Compton kinematics and electron beam characteristics are studied.

The calibration of the CdTe detector, which is to be used to detect X-ray flux for ThomX, was performed using ^{57}Co as a radioactive source.

Chapter One

Introduction

There is a great scientific interest in high flux, monochromatic and energy tunable X-ray sources. These sources are being widely used in various research fields, such as medical, cultural heritage and industrial fields. Synchrotron radiation sources provide high quality X-ray beams that satisfy both monochromaticity and high brightness. The high cost, limited access- time and large size of synchrotron facilities are limitations for users for doing additional research. There is a lot of current research and effort to develop new compact X-ray sources (laboratory size) such as ThomX. The principle of the ThomX source is the production of hard X-rays by the Compton interaction between a relativistic electron bunch and a laser pulse. The ThomX project is designed to provide a compact and tunable energy X-ray source of 70 m^2 surface (1) [1], which could be installed in hospitals, museums, universities or industry factories. Some powerful experimental techniques developed at synchrotron facilities could be transferred to this more compact machine. ThomX is a French project, which will be installed at the Paris-Sud Campus by the end of this year (2018) (Figure 1.1).

The capability of accurately studying the spectral and angular characteristics of a ThomX X-ray beam is crucial for the optimization of the operation of the ThomX as well as for aligning the collimator and experiment apparatus for the application that employs the ThomX Compton X-ray beam. The theory of Compton backscattering of an electron and a photon is limited to the scattering of ideal electron beam and ideal photons pulse, i.e., particle- particle scattering of monoenergetic electron beam and monoenergetic photon pulse (all particles in the same beam have the same energy). However, in reality, the electron and photon beams have finite energy distributions. Therefore, there remains a need to fully understand the characteristics of the X-ray beam produced by Compton backscattering of an electron beam and a photon beam with realistic distributions, i.e., the effect of beam-beam scattering (not all particles in the same beam have the same energy). For this aim, two approaches have been performed, an analytical calculation method and a CAIN based- Monte Carlo simulation technique [2]. Using these two approaches, the ThomX X-rays beam was characterized with varying electron beam parameters as well as different collimation conditions. Based upon the CAIN simulation, to study the energy distribution of the X-rays beam, it is important to know the nominal ThomX electron beam energy spread and normalized emittance which are used in the Compton collision.

Also, during my internship, an energy calibration for the CdTe detector (which will be used in ThomX) was performed by using a radioactive ^{57}Co and when the CdTe detector is located at a fixed distance from the interaction point, the number of X-rays photons striking the detector surface per second is estimated.

a) b)

Figure 1.1: a) The ThomX project on the Université de Paris Sud campus [3]. b) The ThomX will be constructed in the building called IGLOO.

1.1 Motivation of this Work

This section delineates the motivations and the guidelines for the development of a compact machine, aimed at constituting the ThomX project which is being designed to produce a high flux and tunable X-rays beam, which can be easily tuned by changing the electron beam energy. For instance, an electron beam energy tunable in 50-70 MeV ranges provides X- rays with energy 45- 90 keV. The favorable characteristics of the ThomX X-ray source such as a good quality of X-ray beam of small energy bandwidth and monochromaticity make ThomX attractive for a wide spectrum of applications.

The focus on enabled applications by the ThomX due to the expected high flux is on medical oriented research or studies, mainly in the radio-diagnostics and radiotherapy fields, exploiting the unique features of the ThomX monochromatic X-rays on material studies, crystallography and X-ray diffraction. These performances of the ThomX allow the replacement of a conventional X-ray source and huge synchrotrons.

1.2 Outline of Thesis

This thesis is divided into six chapters that explore the studies and simulation aspects that were performed for ThomX. Also the theoretical models of beam parameters which are used in the simulation code are described in detail. In Chapter 2, an overview of the Compton backscattering theory and Compton cross section are introduced and followed by relevant electron beam and laser parameters and their definitions. The energy of a Compton X-ray photon for ThomX ideal electron and laser beams' parameters is calculated (without considering the X-ray beam collimation condition and real beams parameters effects). Based upon Compton cross section, the ideal X-rays spatial and spectral characteristics distribution is studied. In Chapter 3, the calibration of a CdTe detector which will be used in the ThomX has been performed by using a ^{57}Co radioactive source and the obtained measured spectrum has the structure of a full energy peak, Compton edge, escape peaks, florescent X-ray and sum peaks. In Chapter 4, by considering real incoming electron beam parameters, two methods are performed to study their effects on the spectral and angular flux of X-ray beam, one based on analytical formulas and the other based on the CAIN simulation program [2]. Analytical formulas are studied in two cases, the first is without the effect of X-ray beam collimation conditions and the second is with collimated conditions effects. In Chapter 5, the number of Compton X-rays per unit time that enter the surface of CdTe detector located at specific position from the interaction point is calculated through two different methods. The first method is by using theoretical equations to determine the spectral and spatial flux of Compton X-rays. The second one is by using the CAIN program. Finally, in Chapter 6, the conclusion of this thesis is presented.

1.3 Objectives

This thesis highlights spectral and spatial properties of an X-ray Compton beam. It also presents a calibration of a detector which will be used in the ThomX X-ray beam line.

This thesis has two main objectives which are summarized as follows:

- The ThomX X-ray flux and how it is affected by electron beam parameters is studied in details; such as changing electron-beam-normalized emittance, electron beam size and divergence, in order to optimize these parameters to get the highest X-ray flux within a given energy bandwidth and a given angular aperture.
- A CdTe detector which will be used in the ThomX X-ray beam line is calibrated by using ^{57}Co radioactive source. Also, the number of X- ray photons striking the 3mm × 3mm CdTe detector surface area

detector per second is estimated, when the CdTe detector is located at a fixed distance from the interaction point.

1.4 ThomX Hard X-Rays

X-rays are an electromagnetic radiation, just like radio-waves, microwaves, gamma rays and visible light. The only difference between these types of radiation is the wavelength. This thesis will only consider a part of the electromagnetic spectrum referred to "Hard X-rays" whose energy ranges from 10 keV-100 keV, since the ThomX project will produce hard X-ray photons with energy of 45 keV (because of specified parameters chosen for the electron beam and laser pulse). Hard X-rays can be used to reveal internal structure and material properties in a wide range of applications and various fields (as material science, cultural heritage, industry and medicine) due to their ability to penetrate objects.

1.5 Set Up and General Layout of ThomX

At ThomX, the electron beam is composed of one electron bunch, this bunch comprised of billions of particles traveling together at a speed closed to the speed of light (0.99995c). A 50 MeV electron bunch of one nano-coulomb (1nC) with transverse size of the order of a few tens of μm and a divergence of the order of the mrad is in use. The ThomX machine will produce X-rays with a flux rate of 10^{11} - 10^{13} ph/sec [4, 5], and an energy of a few tens of keV.

In ThomX, the electron bunch, confined in a storage ring, collides with a laser pulse at each turn around the ring. The benefit of a storage ring instead of a linear accelerator (LINAC)-based Compton source is that the electron beam can be used multiple times to produce high Compton photons flux instead of only once. In a linear accelerator, the particles see the accelerating field only once (the particles which didn't interact are lost). Because of that, a linear accelerator will have much lower overall flux (each time, new particles should be produced to be accelerated). However, in the use of storage ring, the particles feel the accelerating field each time they turn around and the particles remain in the accelerator for many hours.

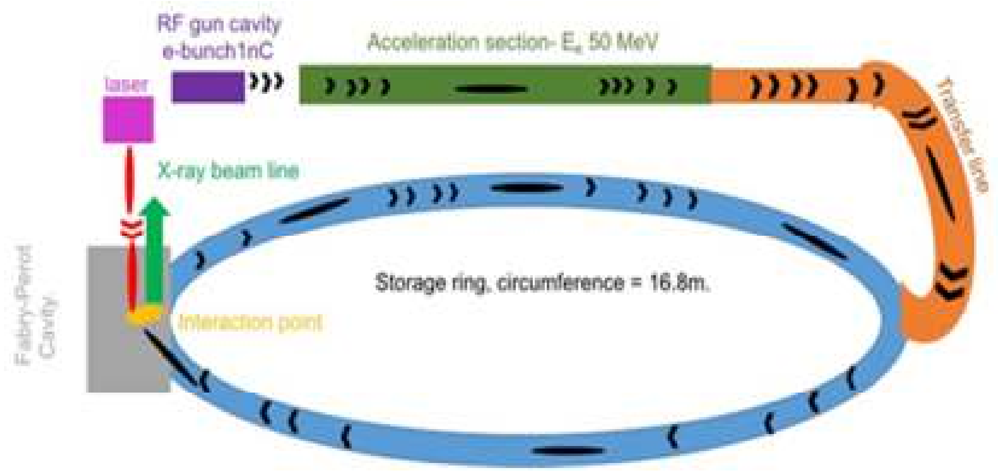

Figure 1.2: Schematic process diagram of the ThomX source. The laser interacts with electrons via the Compton backscattering to produce X-ray photons [5].

The ThomX project is composed of eight main components [4] as shown in Figure 1.2:

- The electron gun delivers one electron bunch of one nano-Coulomb (1nC) each 20-50ms.

- The acceleration section (LINAC) boosts the electron bunch energy up to 50 MeV.

- The transfer line transports the electron bunch from the LINAC to the storage ring. Its length is 14m.

- The storage ring has circumference of 16.8m and a revolution frequency is 17.8 MHz. In the storage ring, the electron bunch is forced to follow a circular motion under the influence of magnets placed along its circumference. The storage ring consists of an array of eight magnetic dipoles that are used to bend the electron bunch, twenty four quadrupoles that are used to focus the electron beam (act as an optics lens) and twelve sextupoles used to correct for chromatic aberration [4].

- Laser: A laser of 1W average power is used. The laser photon energy is 1.16 eV.

- The Fabry- Perot cavity is integrated between two dipoles. The laser power is amplified by accumulating the pulses in a high gain four mirror Fabry-Perot resonator.

- The interaction point is the position where the collision between an electron bunch and a laser pulse occurs to produce Compton X-rays.

- The X-ray beam line has equipment that ensures the detection, the monitoring and the measurement of the X-ray beam flux. Measuring the Compton X-ray beam flux can be accomplished by using a cadmium telluride (CdTe) detector.

ThomX parameters' values, of its three main components, the storage ring, the laser and the Fabry-Perot cavity, are summarized in Table 1.1.

Table 1.1: ThomX parameters values of the Injector, Ring and Laser [1, 4]

Laser pulse energy	30 mJ
Laser wavelength	1066.8 nm
Circumference	16.8 m
Beam current	17.8 mA
Laser Fabry-Perot cavity frequency	35.68 MHz

The electron beam, produced by the gun, is accelerated up to 50 MeV by the LINAC then the electron beam is transferred to the storage ring through the guidance of the transport line. The beam is stored in the storage ring with 17.8 MHz repetition frequency.

Concurrent with the electron beam production, a laser pulse of wavelength λ_L of 1066 nm with a frequency of 35.68 MHz is injected and amplified in an optical resonator and then by a Fabry-Perot cavity. Once the synchronized collisions between an electron bunch and laser occurs, X-rays are produced via Compton backscattering. X-rays are extracted from the interaction point to the X-ray line and the end station.

1.6 Literature Survey

A large number of studies have been carried out by various groups of investigators to measure the X-rays backscattering for different energies of the interacting electron beam and laser pulse. This literature survey has been carried out using available publications in scientific journals related to Compton X-rays (compact X-rays sources) and related to detectors which will be used to detect hard X-rays at the beam line end-stations in ThomX. The research group of E. Frank et al. [6] has studied a compact tunable, monochromatic X-rays source that delivers hard X-rays of energies from 10-50 keV at narrow band width (1-10%), with a flux of 10^{10} photons per 8 ps pulse.

Lattice design of a compact storage ring X-rays source at electron beam energy of 45 MeV has been discussed by A. Poseryaev et al. [7]. Quasi- monochromatic X-rays radiation is produced in the process of Compton backscattering of laser photons by counter propagating relativistic electrons. According to Poseryaev, when 45 MeV electrons interact with a laser pulse of wavelength λ_L equals to 10^{-6} m, the energy spread σ_e is 0.016 and the normalized transverse emittance ε_N is 3×10^{-8} mm.mrad which corresponds to the electron beam size x_e which is equal to 3μm.

Studying Compton backscattering X-rays is performed either by using Monte Carlo simulations or analytical methods. Analytical approaches, provided by M. Jacquet and C. Bruni [2], result in analytic formulas for the angular and the spectral X-ray fluxes. These fluxes are established as functions of the energy spread and the angular divergence of the electron and the laser beams. The detailed predictions of M. Jacquet and C. Bruni are compared with Monte Carlo simulations. These analytic expressions allow one to compute in a simple and precise way the X-ray flux in a given angular acceptance and energy bandwidth, knowing the characteristics of the incoming beams. Monte Carlo simulation work was carried out on Compton scattering studies, where C. Bruni et al. [5] have performed simulations as a function of the electron energy (5, 50 and 150 MeV). According to [5], beam dynamics simulations have been performed for optimizing the emittance and the longitudinal phase space for the storage ring. The ThomX Technical Design Report, published by A. Variola et al. [4] describes the basics of the Compton backscattering effect and gives a first estimation of the ThomX performances based on simulations. These simulations lead to precise predictions concerning the incoming X-ray flux.

Chapter Two

Theoretical Background

In this Chapter, the Compton backscattering theory is reviewed and applied to study the Compton kinematics process in the laboratory frame. First, for ideal incoming beams, the backscattered photon energy is calculated as a function of scattering angle. Also, the Compton scattering cross section is introduced with ideal beams interacting. Then, the real electron beam characteristics (energy spread, beam divergence, normalized emittance and bunch length) are described. Finally, the interaction between real electron beam and laser pulse and their effect on the scattered photons energy broadening is introduced.

2.1 Compton Backscattering

To have a good estimation of the ThomX performance, an overview of the Compton backscattering principle is provided. The theory of Compton backscattering of an electron and a photon is limited to the scattering of ideal electron beam and ideal photons pulse (like particle-particle monoenergetic electron beam and monoenergetic photon pulse).

2.1.1 Kinematics of Compton backscattering

The Compton scattering process between a photon of energy E_L and an electron of energy E_e in the laboratory frame is shown schematically in Figure 2.1.

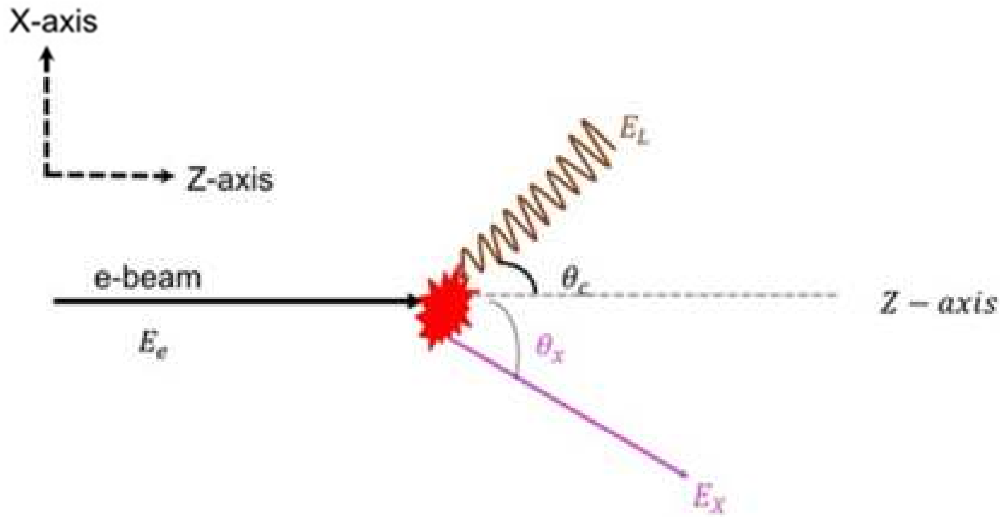

Figure 2.1: Scheme of the interaction between an electron and a photon. E_e is the energy of the electron beam (50MeV for ThomX), EL is the energy of the incident laser photon, and θ_c is the incident laser angle with respect to electron beam direction and E_x is the energy of the X-ray scattered photon and its scattering angle is θ_x with respect to the electron beam direction.

In the laboratory frame and using total energy conservation and linear momentum conservation, it can be shown that the energy of the scattered photon E_x [1, 2, 4, 5, 8] is given by:

$$E_x = \frac{2\gamma^2 E_L(1+\cos\theta_c)}{1+\gamma^2\theta_x^2} \tag{2.1}$$

Where θ_c is the incident laser angle with respect to electron beam direction, θ_x is the scattering angle with respect to the electron beam direction and γ is the ratio of the electron energy to its rest mass (for ThomX: E_e=50 MeV, γ =100), E_L is the energy of laser photon and we define $E_m=2\gamma^2 E_L(1 + \cos\theta_c)$ as the maximum energy of the scattered photons which is emitted on-axis (θ_x=0°).

The energy of scattered X-ray photons have a quadratic dependence on the electron energy (γ^2) [5]. The maximum energy of the scattered photon for head-on collisions (E_x=45 keV for E_e=50 MeV, E_L =1.16 eV and θ_c=0°) will be obtained when the scattering angle θ_x is zero.

Equation 2.1 shows a univocal dependence of the X-ray energy on its scattering angle. That is, the X-ray energy has one single value at a given scattering angle. This is very effective for selecting the energy and consequently to obtain a quasi-monochromatic beam. A lower energy scattered photon corresponds to a photon with a larger scattering angle with respect to the electron beam direction. Equation 2.1 shows that, with θ_c=0°, the scattered photons having half of the maximum energy $E_m/2$ are scattered at an angle equal to $1/\gamma$. For ThomX, we can obtain the value of the scattering angle θ_x equal to 10 mrad (which corresponds to $1/\gamma$ =1/100), for the X-ray photon with an energy of 22.5 keV (which is half of the maximum X-ray photon energy of 45 keV) as shown in Figure 2.2. Figure 2.2 shows the obtained dependence from Equation 2.1 between the Compton photon energy and scattering angle in the case of an ideal electron beam and an ideal laser beam (particle-particle interaction, all particles in the same beam travel in the same direction and have the same energy).

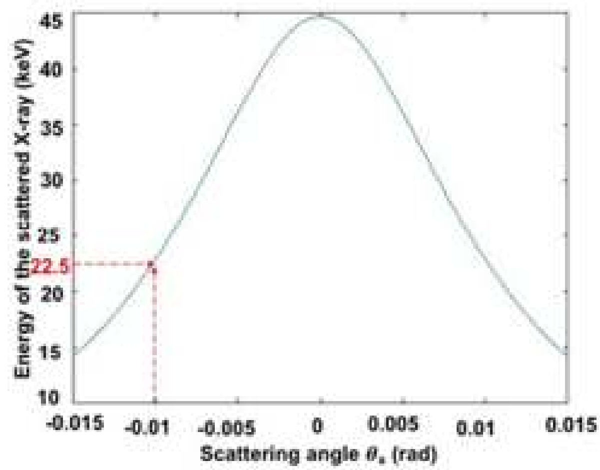

Figure 2.2: Dependence obtained between the Compton X-ray energy and the scattering angle. X-ray photons are produced from the interaction between an ideal (particle-like) electron beam of 50 MeV through head-on collisions with an ideal 1060 nm laser pulse via Compton backscattering. Photons of maximum energy 45 keV are on-axis. X-rays photons with energy 22.5 keV scattered at angle of 10 mrad (which corresponds to $\theta_X = 1/\gamma, \gamma = 100$ for ThomX).

Compton radiations are emitted in a forward cone with respect to the electron beam direction (Figure 2.3). For a 50 MeV electron beam energy, the radius of a cone is 10 cm at the distance of 10 m from the interaction point. The cone radius depends on the electron beam energy and the position where the radius is measured with respect to the interaction point.

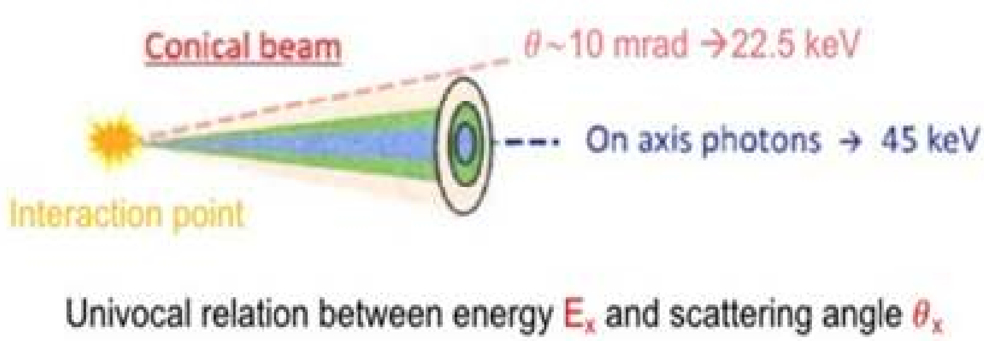

Figure 2.3: Compton radiation is emitted within a cone along the electron beam trajectory [8]. For E_e = 50MeV, E_L = 1.16 eV and θ_C=0°.

2.1.2 Compton backscattering cross section

The normalized differential Compton cross section (P_{Ex}) with respect to the ratio of X-ray energy E_x and E_m was derived by Telnov who obtained the expression [2, 8]:

$$P_{Ex} = \frac{3}{2}\left[1 - 2\varepsilon + 2\varepsilon^2\right] \qquad (2.2)$$

where $\varepsilon = \frac{E_x}{E_m}$ and $E_m = 4\gamma^2 E_L$; for $\theta_c = 0°$

The significant dependence of the differential cross-section of a Compton scattering on the initial energy of ideal electron beam, ideal laser pulse energy and the incident angle should be noted.

By using Equation 2.2, the differential cross section (P_{Ex}) dependence on the energy of scattered X-ray photons for an ideal laser pulse (λ = 1060 nm) and an ideal electron beam (E_e =50 MeV) in a head on collision, is obtained and represented in Figure 2.4.

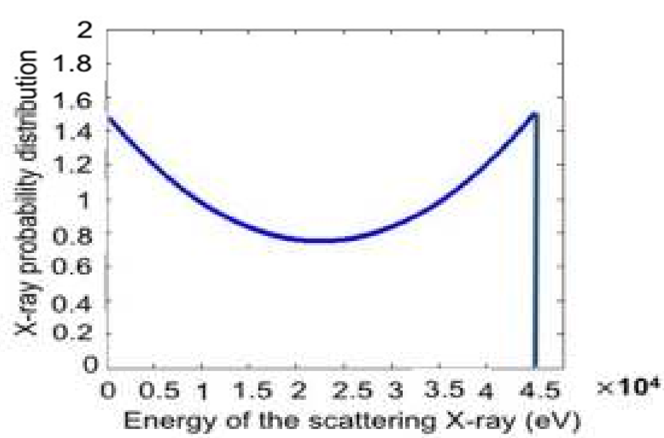

Figure 2.4: The differential cross-section P_{Ex} as a function of backscattering X-ray energy for head-on-collisions of an ideal 1060 nm laser beam with an ideal electron beam of 50 MeV.

2.2 Beam Dynamics

The beam dynamics theory and its associated notations is discussed in this section starting with the definition of the basic coordinate system that is often use to describe the motion of the billions of particles that comprise each bunch.

2.2.1 Coordinate system used for accelerator particles

In ThomX, billions of electrons travel together in group as a 'bunch' in a dominant direction. A theoretical particle that travels along the ideal beam path at the average energy of the bunch could be considered as the "synchronous particle".

It is useful to define the coordinate system that describes any given particle's position and velocity relative to that of the synchronous particle. The s-direction is the particle's longitudinal motion, p_s is the longitudinal momentum of the particle, x and z are the transverse coordinates. A sample coordinate system is shown in Figure 2.5. A particle, during its transverse motion in an accelerator, is characterized by its position s or displacement from the central orbit x and its angle with respect to the central orbit θ ($\theta = x' = dx/ds$), as shown in Figure 2.6.

Figure 2.5: Coordinate system used for accelerator particles. The particle bunch moves in the s direction, while x and z are the transverse directions.

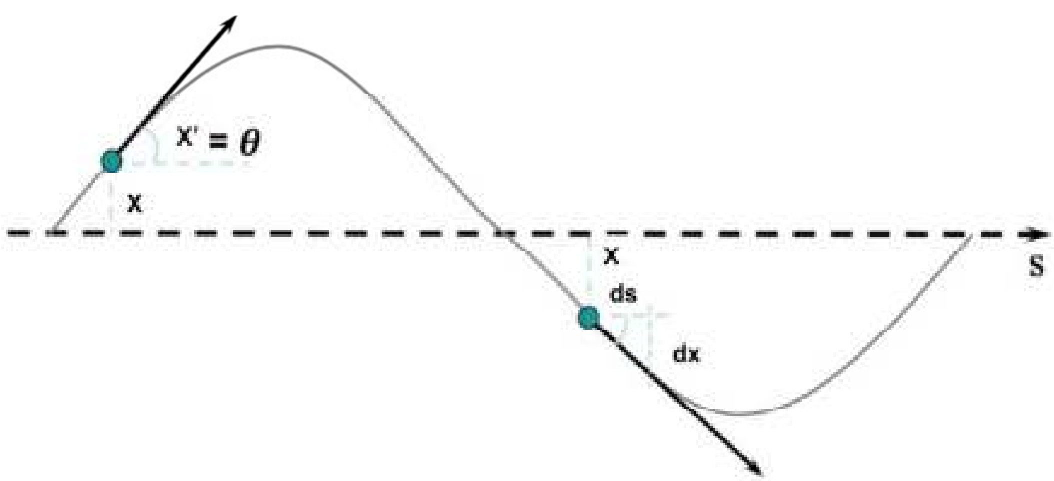

Figure 2.6: The particle position from the central orbit and its deviation angle with respect to the central orbit. Where s is the longitudinal displacement around the ring, x is the transverse displacement and x' is the angle with respect to the central orbit angle with respect to the central orbit and it equals to dx/ds.

If we plot x' versus x we get an ellipse, which is called the phase space ellipse.

The synchronous particle travels along the ideal path through the particle accelerator. The traveled distance is denoted by s, and it is common to describe various parameters as a function of s.

2.2.2 Electron bunch size

The betatron function is denoted by $\beta(s)$ for the electron bunch at the location s along the nominal beam trajectory. It is a generalized measure of the beam size and it is defined by the envelope that contains the particles through motion. The betatron function and the beam's transverse emittance (ε) are related to the bunch size x_e which is defined by Equation 2.3.

$$x_e = \sqrt{\beta(s)\varepsilon} \qquad (2.3)$$

This expression neglects the small contribution from the electron beam energy spread in the Equation that gives x_e which is written as Equation 2.4.

$$x_e = \sqrt{\beta(s)\varepsilon + [D(s)\sigma_e]^2} \qquad (2.4)$$

where D(s) is the dispersion function. The transverse emittance (ε) is the area of the phase-space ellipse, which is invariant and it has the dimension of length times angle (m.rad). The bunch size is the phase space ellipse projection along the x-axis as shown in Figure 2.7.

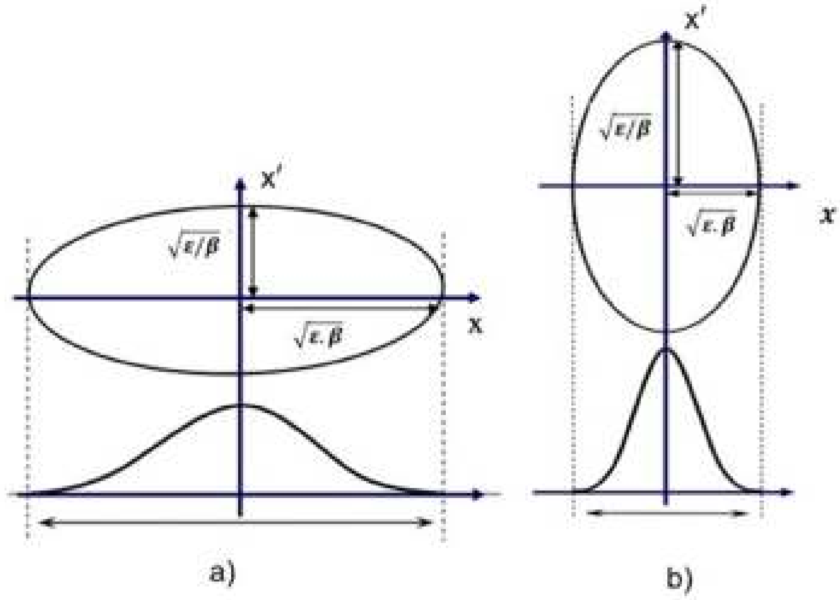

Figure 2.7: Each point inside the ellipses corresponds to x, x' values of a single particle. The projection of the ellipse on the x-axis gives the transverse beam size [9]. The variation of β (s) around the machine will tell us how the transverse beam size will tell us how the transverse beam size will vary (the difference between a) and b)).

2.2.3 Electron beam energy spread

The energy of electrons within a bunch is not fixed for all electrons. Each of the billions of particles has its own relative motion and energy. Some electrons have energy higher than the synchronous electron energy and some have lower energy. Assume that the energy of the electrons in the beam follows a Gaussian distribution with a mean energy E_e and a standard deviation σ_E , then the energy spread is defined as $\sigma_e = \sigma_E$ (Figure 2.8-a).

This energy spread gives rise to the electron bunch length (z_e) because electrons with higher energy than the synchronous particles will be at the head of the bunch, while electrons with lower energy than the synchronous particles will be at the tail of the bunch as shown in Figure 2.8-b.

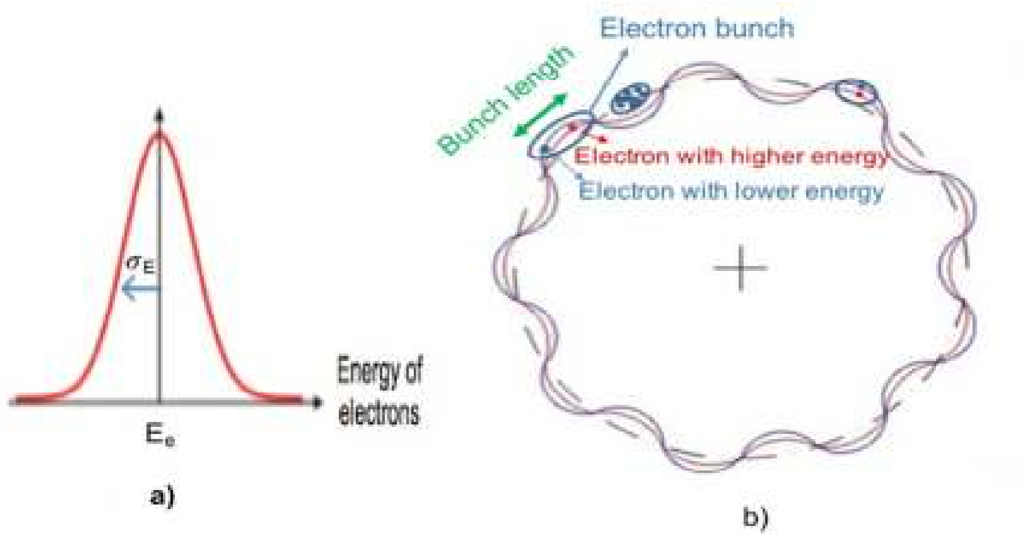

Figure 2.8: a) A Gaussian distribution of electron beam energy spread with standard deviation σ_E and mean energy E_e. b) Electrons with energy higher than the one of synchronous electron is at the head of the bunch while electron with lower energy than the one synchronous electron is at the tail of the bunch, this energy spread causes the electron beam bunch length [10].

2.2.4 Divergence of the electron beam trajectory

The electron beam divergence (σ_e') is the angular measure of the increase in the electron beam diameter with distance from the optical aperture from the electron gun. It is measured in radians (rad). For many applications, a low divergence is needed to get a good beam quality.

Emittance is a property of a particle beam that characterizes its size and its divergence. For an electron beam, the normalized emittance is related to the beam transverse size (x_e), the beam divergence (σ_e') and the beam energy (E_e). It is given by Equation 2.5.

$$\varepsilon_N = \gamma \sigma_e' x_e \tag{2.5}$$

where γ is Lorentz factor ($\gamma = \frac{E_e}{m_0 c^2}$), and m_0 is the electron rest mass).

Once an electron bunch is produced by an electron gun, its normalized emittance remains constant all over an acceleration. Since the normalized emittance is invariant for an electron beam, the transverse size can be related with the divergence and vice versa. Hence, a decrease in the divergence σ_e' of thebeam causes an increase of the transverse size x_e. The emittance and the energy spread of the electron beam plays an important role in the quality of a Compton source.

2.3 Beam-Beam Interacting (Real beams)

Scattered X-ray photons are not generated by a single particle, but rather by an electron beam which interacts with a laser pulse with a non-zero angular divergence and non-zero energy spread (beam -beam interacting). The angular divergences (σ_e', σ_L') and the energy spreads (σ_e, σ_L) of the electron bunch and the laser pulse, respectively, at the interaction point lead the scattered X-rays to have different values of energy at the same scattering angle θ_x. These incoming beam parameters lead to a significant broadening of the energy-angle distribution presented in Figure 2.2.

In most of practical cases, the divergence and the energy spread of the laser pulse produces a negligible effect on the X-ray spectrum broadening. Hence, we consider in the following only the effects due to the incoming electron beam (energy spread and beam divergence).

• The X-ray energy spectral broadening ($\frac{\Delta E_x}{E_x}$) due to the electron beam energy spread (σ_e) and by using Equation 2.1 [2], can be expressed as:

$$\frac{\Delta E_x}{E_x} = 2\sigma_e \tag{2.6}$$

This can be shown by replacing γ with γ ($1+\sigma_e$) in Equation 2.1.

$$\frac{\Delta E_x}{E_x} = \frac{\frac{2\gamma^2(1+\sigma_e)^2 E_L(1+\cos\theta_c)}{1+\gamma^2\theta_x^2} - \frac{2\gamma^2 E_L(1+\cos\theta_c)}{1+\gamma^2\theta_x^2}}{\frac{2\gamma^2 E_L(1+\cos\theta_c)}{1+\gamma^2\theta_x^2}} \tag{2.7}$$

By using Taylor expansion of $(1 + x)^2 = 1+2x+...+...$, the term $(1 + \sigma_e)^2$ can be expanded and approximately equal to ($1 + 2\sigma e$), then Equation 2.7 can be written as:

$$\frac{\Delta E_x}{E_x} = \frac{\frac{2\gamma^2(1+2\sigma_e) E_L(1+\cos\theta_c)}{1+\gamma^2\theta_x^2} - \frac{2\gamma^2 E_L(1+\cos\theta_c)}{1+\gamma^2\theta_x^2}}{\frac{2\gamma^2 E_L(1+\cos\theta_c)}{1+\gamma^2\theta_x^2}} = 2\sigma_e \tag{2.8}$$

The energy spectral broadening of the backscattered X-rays due to the electron beam energy spread is twice the electron beam energy spread ($2\sigma_e$).

• The X-ray spectral energy broadening due to the divergence of the electron beam (σ_e') [2] can be given by Equation 2.9.

$$\frac{\Delta E_x}{E_x} = \gamma^2 \sigma_e'^2 \tag{2.9}$$

This equation can be derived by replacing θ_x by σ_e' in Equation 2.1.

$$\frac{\Delta E_x}{E_x} = \frac{\frac{2\gamma^2 E_L(1+\cos\theta_c)}{1+\gamma^2\sigma_e'^2} - \frac{2\gamma^2 E_L(1+\cos\theta_c)}{1+\gamma^2\theta_x^2}}{\frac{2\gamma^2 E_L(1+\cos\theta_c)}{1+\gamma^2\theta_x^2}} \tag{2.10}$$

For a head on-axis X-ray photons $\theta_x = 0°$, then Equation 2.10 can be expressed as $\frac{\Delta E_x}{E_x} = \gamma^2 \sigma_e'^2$.

For instance, for a 50MeV electron beam with divergence of σ_e' 1mrad leads to X-ray beam relative energy spread $\frac{\Delta E_x}{E_x}$ of 1% and with electron divergence of 2 mrad leads to $\frac{\Delta E_x}{E_x}$ of 4%.

Equations 2.6 and 2.9 are important for the study of the X-ray energy versus X-ray scattering angle where they are result in spectral broadening of X- rays vertically (different X-rays energies at the same scattering angle) and horizontally (different X-rays scattering angles at the same energy).

Chapter Three

Calibration of Cadmium Telluride Detector

Some theoretical background of semiconductor detectors will be introduced, then an overview on the interaction process between photons and matter (photoelectric interaction, Compton scattering and pair production) will be provided. Finally, a calibration for a detector that will be used in the ThomX has been performed by using a radioactive source. After that, the spectrum components (photopeaks, Compton edge, X-ray florescent, escape peaks and sum peaks) for this radioactive source are identified.

3.1 Semiconductor Detector

In semiconductor detectors, incident radiation on a semiconductor crystal generates electron-hole pairs which are collected with an applied electric field and result in an electrical signal. The number of electron hole pairs generated is proportional to the energy of the incident radiation, so the spectroscopic information of the incident radiation could be obtained.

In ThomX, the backscattered X-ray photons have a maximum energy in the range from 45 keV to 90 keV (E_e = 50 MeV - 70MeV). Therefore, a CdTe detector is the best suitable detector for detection of the X-ray beam line in ThomX because it has high absorption efficiency up to 100 keV [11]. A high energy backscattering X-ray photon is a limiting factor for Si detectors. Si detectors are only effective for absorbing photons of energies up to 30 keV as the absorption efficiency decreases above this value due to its low atomic number (Z=14). In order to avoid this limitation, semiconductor materials of higher atomic number such as Ge and CdTe could be used. Ge detectors have an excellent energy resolution in the energy range between 1 keV and 1 MeV. The limitation to use Ge detectors is that Ge has a small band gap of 0.67 eV at room temperature [11]. At room temperature, a small band gap results in the generation of a large number of the thermal carriers. In order to overcome this limitation, Ge detectors must have a cryostat system.

In ThomX, CdTe detector of 3mm × 3mm surface area will be used because it is an excellent choice for room temperature X-ray spectroscopy and due to its good detection at high energies (more physical properties for CdTe are listed in Table 3.1). Where the electrons' mobility (μ_e) and the hole's mobility (μ_h) characterize how quickly an electron or a hole can move through a metal or semiconductor, when it pulled by an electric field.

Table 3.1: Physical properties for CdTe [11]

Atomic number	Cd= 48 and Te= 52	
Density	6.2	gm/cm^3
Band gap	1.44	eV
Pair creation energy	4.43	eV
$\mu_e\tau_e$	10^{-3}	cm^2/V
$\mu_h\tau_h$	10^{-4}	cm^2/V

Testing the CdTe detector, which will be used in ThomX is performed by using peaks of a known source; we use a known radioactive source (^{57}Co) which produces discrete gamma energy lines at 14.4, 122, and 136 keV (Figure 3.1-a).

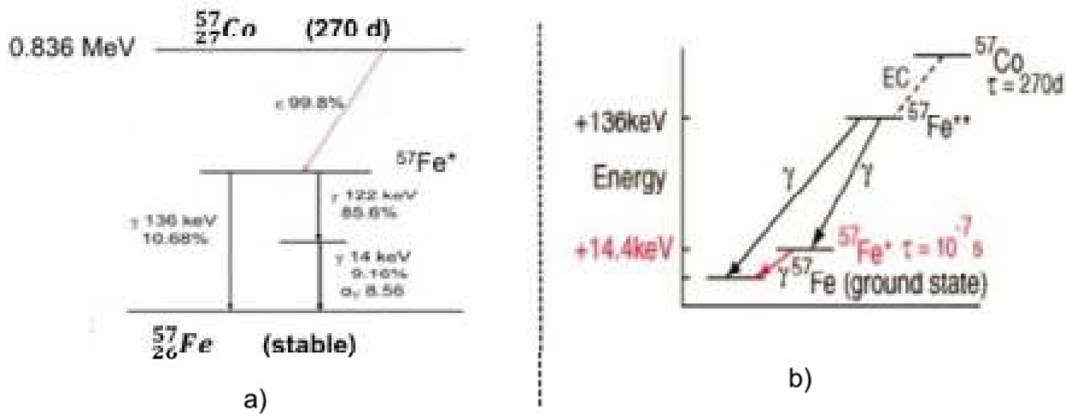

Figure 3.1: a-) Cobalt-57 decay scheme. b-) Scheme for ^{57}Co produces ^{57}Fe in an excited state [12].

Table 3.2: Physical data for cobalt-57 [13]

Photon energy	136keV (11%) 122 keV (86%) 14.4 keV (9%)
Half-life time	270.9 days
Specific activity	8.481×10^{3}Ci/gram

Table 3.2 summaries information about the peaks that are identified in the spectrum of the radioactive source ^{57}Co. The decay of ^{57}Co by electron capture produces an excited state of ^{57}Fe. The electron capture process changes a proton of ^{57}Co to a neutron that forms an excited state of the ^{57}Fe nucleus. The exited state of ^{57}Fe emits photons in order to reach the ground state (Figure 3.1-b) (Table 3.3).

Table 3.3: Physical data for iron-57 [13]

X-ray emission lines (K_{α} & K_{β})	Energy (keV)	Relative probability
$K_{\alpha 2}$	6.39	5.07%
$K_{\alpha 1}$	6.40	100%
$K_{\beta 2}$	7.05	20.66%
$K_{\beta 1}$	7.05	20.66%

Radiation detectors' operating mode depends on the mechanism of radiation interaction with the material which is composing the detector. Gamma rays interact with matter in three ways; first of all, photoelectric absorption; secondly, by Compton scattering; finally, through pair production. These three interactions make different contribution to the measured energy spectra

as shown in Figure 3.2.

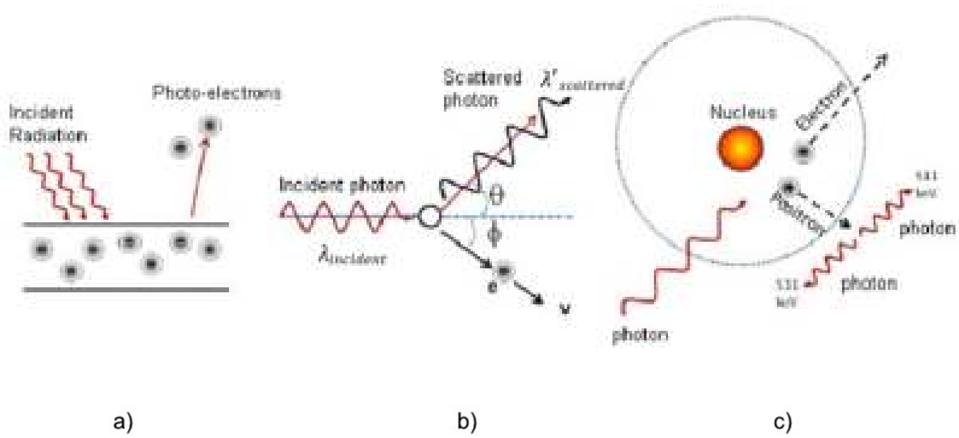

Figure 3.2: a) Photoelectric effect. b) Compton scattering. c) Pair production [14].

a. Photoelectric effect:

The photon energy is completely absorbed in the matter, supplying enough energy to release an electron from the bound state. The kinetic energy of an ejected electron ($K.E_e$) is given by [15]:

$$K.E_e = E_\gamma - E_b \quad (3.1)$$

where E_γ is the energy of the incident photon and E_b is the binding energy of the electron. In the ideal case, in which there is only a photoelectric process and the gamma ray is completely absorbed in the ideal detector, we will obtain a very sharp full energy photopeak [15]. In the photoelectric effect, the inner-most shell electron in the atom (K- shell) has some probability to be ejected. The ejected electron leaves a vacancy in the shell. An electron from a higher level fills in the K-shell. Since the K-shell is the lowest energy level, the difference in the internal state energy is emitted as a fluorescent X-ray. The energy difference between the two binding energies is a characteristic of the atom, in which the fluorescence process occurs. The emitted fluorescent X-ray is called the characteristic X-ray because it uniquely identifies the element.

b. Compton scattering:

The incident photon is scattered by an electron. Therefore, the incident photon transfers a part of its energy to the ejected electron.

The loss of energy for the scattered photon and the gain of energy for the Compton electron depend on the photon scattering angle θ. The linear momentum and the total energy are conserved. The scattered photon has a longer wavelength λ_0 than the incident photon which has a wavelength λ [15]. From simple computations:

$$\lambda'_{scattering} = \lambda_{incident} + \frac{h}{m_e c}(1-\cos\theta) \tag{3.2}$$

where m_e is the mass of the electron which is equal to 0.511 MeV/c^2 and h is Plank's constant.

Then the energy of the Compton electron is equal to the difference between the initial and the backscattered gamma photon energies:

$$E_e = E_i - E'_\gamma \tag{3.3}$$

where E_i is an energy of the incident photon and E_γ' is an energy of the scattered photon:

$$E'_\gamma = \frac{E_i}{1+\frac{E_i}{m_e c^2}(1-\cos\theta)} \tag{3.4}$$

Two extreme cases are possible:

- The minimum energy transfers to the electron when the scattering angle of the photon is zero ($\Delta\lambda = 0$). It means that the energy of the incident photon is equal to the energy of the scattered photon. In other words, there is no energy transfer to the electron.

- The maximum kinetic energy is transferred to the electron when the photon is scattered through an angle $\theta = 180^\circ$ ($\Delta\lambda$ is maximum $=2\frac{h}{m_e c^2}$).

At the intermediate scattering angle, the amount of energy transferred to the electron must be between those two extremes. The photon that scattered through an angle of 180° is called backscattered photon, and its energy is given by the following Formula [15]:

$$E'_{\gamma\,(backscattered)} = \frac{E_i}{1+2\frac{E_i}{m_e c^2}} \qquad (3.5)$$

c. Pair production:

The incident photon energy creates electron-positron pair. The minimum energy of the incident photon required to produce a pair is twice the electron mass. If the incident photon has energy higher than 1.022MeV [15], the excess energy is given to the electron-positron pair as kinetic energy.

3.2 The Measured Spectrum for the Radioactive Source ^{57}Co with Lead Shielding

In the lab, we carried out an experiment to calibrate the CdTe detector that will be used in the ThomX, by determining its response to a known radioactive source ^{57}Co. This radioactive source is used to confirm the satisfactory operation of this CdTe detector. Also, we have checked the change of CdTe response with respect to the energy of the incident radiation.

A computer program is needed in order to visualize and perform a basic spectrum analysis by using spectrum analysis software. The result is a graph of counts of photons as a function of photon energy. Figure 3.3 is a calibrated spectrum and the photopeaks are marked. The other component (Compton edge and Compton continuum, florescent X-rays, escape peaks and sum peaks) of the spectrum are visualized in Figure 3.4.

In testing the CdTe detector, by taking into account the radiation safety rules, we used a lead shield as radiation protection. Lead can effectively attenuate radioactive source radiation due to its high density and high atomic number.

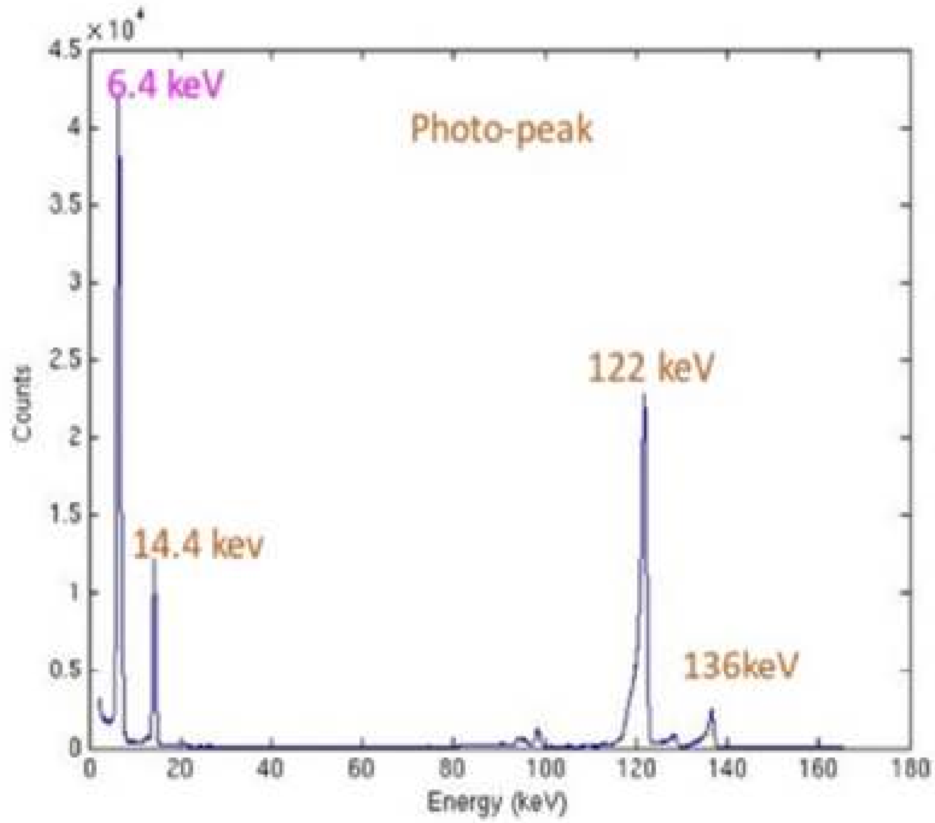

Figure 3.3: ^{57}Co spectrum representing photopeaks.

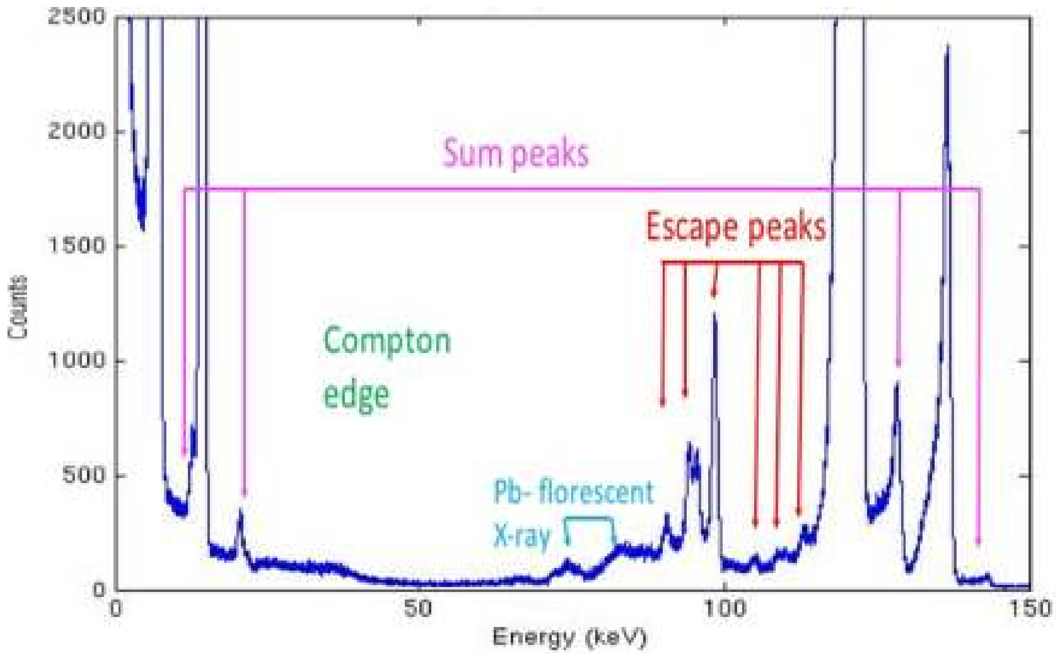

Figure 3.4: The spectrum components of ^{57}Co with lead shielding.

3.2.1 Spectrum components:

The following three photopeaks from ^{57}Co were used for calibration: 14.4, 122, and 136 keV (Figure 3.3). The origin of the unknown peaks on the measured gamma spectrum will be explained.

3.2.2 Full energy peak

A full energy peak appears when an incident gamma ray energy is absorbed completely by the detector. A gamma ray transfers its energy to an atomic electron via the photoelectric effect. This event gives rise to a full energy peak at the energy equal to the gamma energy (Figure 3.5).

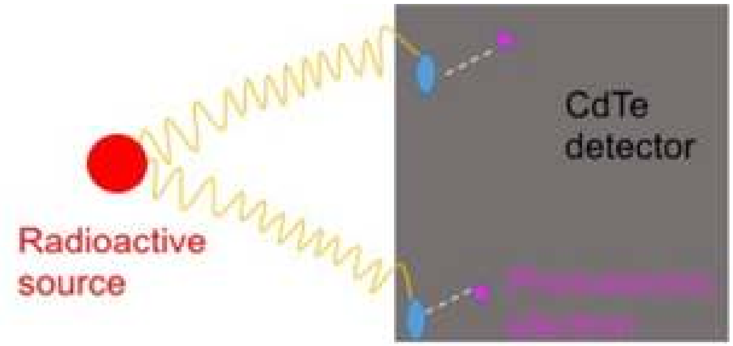

Figure 3.5: Photoelectric interaction of the incident photon with an electron.

The decay of a ^{57}Co nucleus produces a daughter ^{57}Fe in an excited state, which in turn decays to the ground state with emission of X-rays [13]. These X-rays are responsible for the expected peak at 6.4 keV (Figure 3.3). The three measured photopeaks are observed at 14.4, 122 and 136 keV. These peaks correspond to the photoelectric interaction of photons with electrons of the CdTe detector, in which the incident photon energy (14.40, 122.00 and 136.00 keV) is absorbed by the crystal (CdTe). The full energy peak width (Gaussian shape) is determined by the statistical fluctuations of the charges produced from the interactions plus a contribution from the electronics. The Gaussian shape centroid represents the incident photon energy. The photo- peak distribution should be Gaussian. However, at 122 keV and 136 keV, two photopeaks have tails extending toward the lower energies (Figure 3.4), which is due to hole trapping. Hole trapping is responsible for incomplete charge collection in the detector [16]. For the CdTe semiconductor detector, a high probability for recombination of electron and holes exists due to high impurities in CdTe detector. Holes have ten times less mobility than the electrons' mobility and they have a shorter lifetime than the electrons' lifetime (Table

3.1). When the photoelectric interaction occurs inside the detector and far from the detector surface (cathode), the time needed for the holes to reach the cathode is larger than the hole lifetime. In other words, the holes will be trapped and this will produce fewer signals than the expected [16].

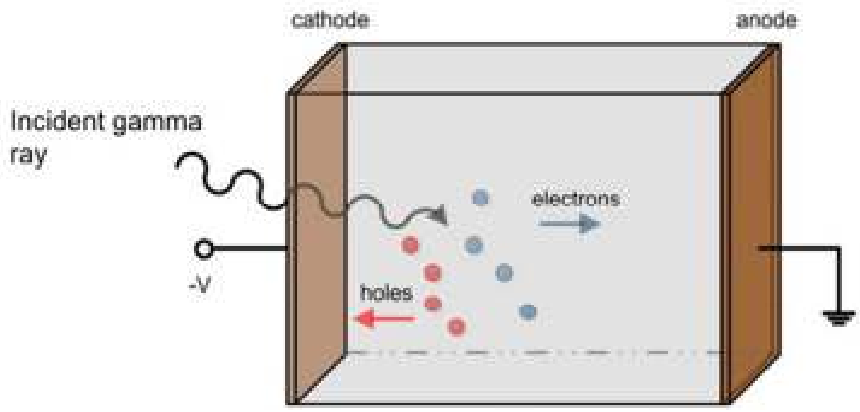

Figure 3.6: Planer configuration of a semiconductor detector. Electron-hole pair are generated by radiation. They are swept toward the appropriate electrode by the electric field [11].

For low gamma ray energies (e.g., 14.4 keV), the photoelectric interaction occurs beneath the surface of the detector (cathode), but the interaction is close to the surface. It means that the time needed for the hole to reach the cathode is less than the hole lifetime. The probability to lose the hole by recombination is very low. Since the electron has higher mobility and larger lifetime than the hole, it will reach the anode without any loss. At higher gamma ray energies (122, 136 keV), the photoelectric interaction occurs everywhere in the detector. If the interaction occurs at a certain depth where the time needed for the hole to reach the cathode is larger than the hole lifetime, the hole will be trapped and results in a signal less than that expected. In conclusion, the fraction and the resultant pulse height depend on the interaction depth (measured from the cathode) and the energy of the incident gamma rays (Figure 3.6).

3.2.3 Compton edge and Compton continuum

When the Compton effect occurs, the scattered gamma escapes from the detector. The detected energy is the kinetic energy given to the ejected electron (Figure 3.7). Depending on the scattering angle, the detected energies vary from the minimum value of the scattering angle ($\theta = 0^{\circ}$) to the maximum value of the scattering angle ($\theta = 180^{\circ}$), and thereby we get the Compton edge. The Compton edge represents the maximum energy loss by the incident photon. Equation 3.5 and Equation 3.3 are used to calculate the energy of Compton edge ($\theta = 180^{\circ}$).

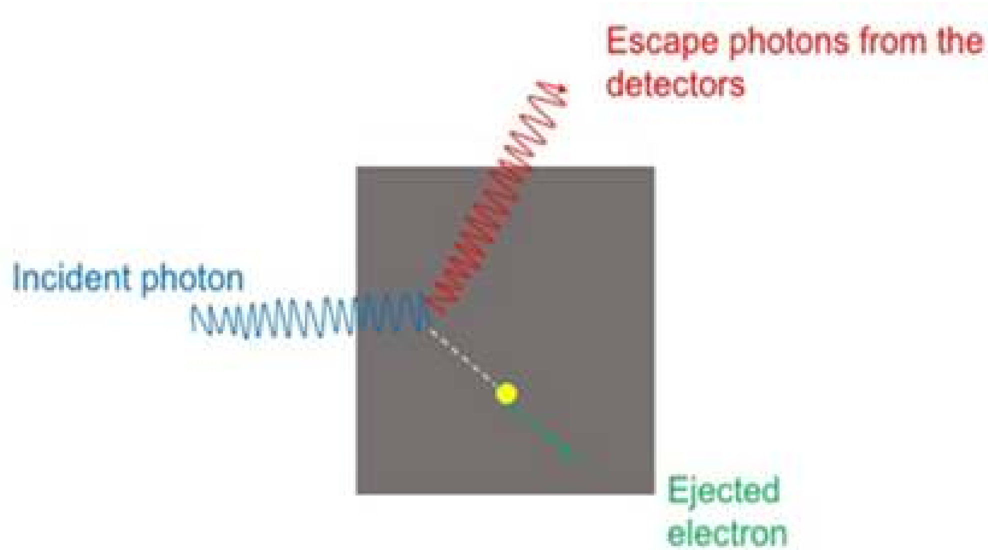

Figure 3.7: Gamma ray interacts with detector's electrons via Compton scattering.

The Compton edge energy for the two incident gamma rays can be calculated:

• For 122 keV incident gamma ray:

From Equation 3.5, the calculated value of energy of the backscattered photon is 82.5 keV.

We get from Equation 3.3 the Compton edge $E_{\text{Compton edge}}$ is at 39.5 keV.

• For 136 keV incident gamma ray:

From Equation 3.5, the expected energy of the backscattered photon is 88.7 keV.

We get from Equation 3.3 the Compton edge $E_{\text{Compton edge}}$ is at 47.3 keV.

The measured spectrum (Figure 3.4) does not show any peak of Compton edge at 47.3 keV, because the intensity 136 keV gamma ray is ten times less than 122 keV gamma ray intensity.

3.2.4 Florescent X-rays

Gamma rays undergo photoelectric interactions with the detector and the material surrounding the detector. There is a probability for this photoelectric interaction to eject an electron from an inner shell of the atom with kinetic energy which is given by Equation 3.1. It results in leaving an electron vacancy in the K-shell. An electron from a higher energy level could fill this vacancy by emitting a characteristic X-ray. As a lead shield surrounds the detector, the photoelectric interaction of incident gamma ray with K-shell electrons from lead will produce Pb- fluorescent X-rays

(Figure 3.8). The result will be a number of X-ray peaks in the measured gamma spectrum in the region between 72 keV and 85 keV (Figure 3.4). Table 3.4 shows the X-ray florescence of lead.

Table 3.4: Florescence X-ray for lead [17]

Energy(keV)	X-Ray Emission line
74.96	$K_{\alpha 1}$
72.80	$K_{\alpha 2}$
84.93	$K_{\beta 1}$

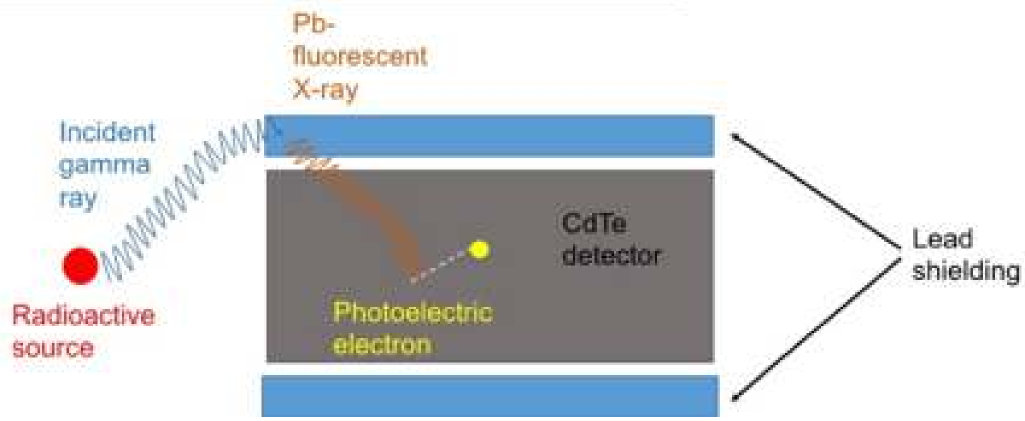

Figure 3.8: Gamma ray interacts with the detector's shielding resulting in Pb-florescent X-ray.

3.2.5 Escape peaks

When gamma rays interact by photoelectric interaction with the CdTe detector, they are able to excite some Cd and Te atoms. During the atom transitions to ground state level, Cd and Te atoms emit a characteristic X-ray at the energies shown in Table 3.5. However, for those events near to the surface of the detector there is reasonable probability that some fluorescent X-rays might escape from the detector. A peak will appear in the gamma ray spectrum at the energy of incident gamma reduced by the K-edge energy of Cd or Te as shown in Figure 3.9.

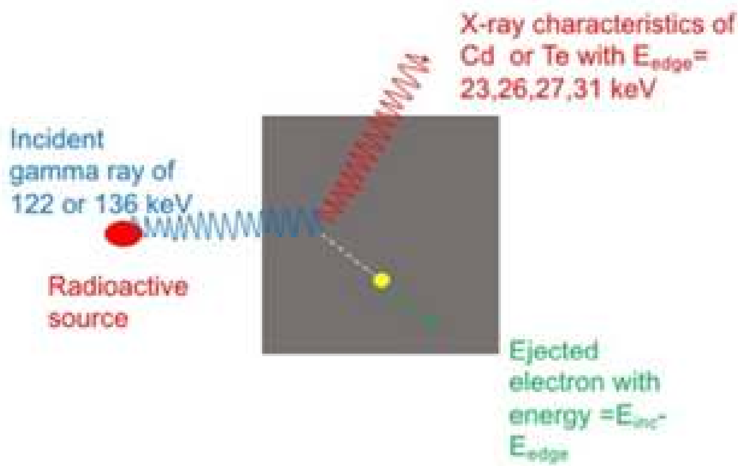

Figure 3.9: Characteristics X-rays escape from CdTe detector.

Table 3.5: Cd and Te X-ray emission lines [17]

Element	$K_{\alpha 1}$ (keV)	$K_{\alpha 2}$ (keV)	$K_{\beta 1}$ (keV)
Cd	23.17	22.98	26.09
Te	27.47	27.20	30.99

The escape peaks for characteristic X-ray for Cd and Te, are expected in the energy range between 91 and 108 keV (Figure 3.4).

The expected escape peaks are:

- 122 keV - 23.17 keV=98.83 keV.
- 122 keV - 22.98 keV=99.02 keV.
- 122 keV - 26.09 keV=95.91 keV.
- 122 keV - 27.47 keV=94.53 keV.
- 122 keV - 27.2 keV=94.8 keV.

- 122 keV - 30.99 keV=91.01 keV.
- 136 keV - 23.17 keV=112.83 keV.
- 136 keV - 22.98 keV=113.02 keV.
- 136 keV - 26.09 keV=109.91 keV.
- 136keV - 27.47 keV=108.53 keV.
- 136 keV - 27.2 keV=108.8 keV.
- 136 keV - 30.99 keV=105.01 keV.

3.2.6 Sum peaks

When two or more photons reach the CdTe detector simultaneously, the electronic circuit cannot distinguish two signals. Only one single pulse is recorded. This event forms a peak which is called a sum peak. The peak energy corresponds to the sum of energies of the two photons. These sum peaks are not only obtained from events of the same element, but also from events of different elements. The excited ^{57}Fe emits an X-ray with energy at 6.40 keV with a probability of 100%. This 6.40 keV X- ray is responsible for the sum peaks on our measured spectrum.

We expected to have sum peaks at: 12.8 keV (6.40 keV+6.40 keV), 20.8 keV (14.40 keV+6.40 keV), 128.4 keV (122 keV+6.40 keV), and 142.4keV (136keV+6.40 keV) (Figure 3.4).

It must be noted that there are no annihilation peaks on the spectrum. This is exactly what is expected, since the emitted gamma rays of radioactive ^{57}Co are not energetic enough (1.002 MeV) to undergo pair production.

Chapter Four

Simulation Results of Angular and the Spectral Flux of the ThomX Source

In Chapter 2, the spatial and energy distributions of a Compton X-ray beam using the (particle-particle) scattering theory was studied. In this theory, an ideal electron and laser beams with zero energy spread and zero divergence were assumed. However, in the reality, electron and laser beams have finite spatial and energy distributions, which could affect the X-rays beam energy distribution. Therefore, there remains a need to study the characteristics of the X-rays beam produced by Compton backscattering of a real laser beam and a real electron beam, i.e., the (beam-beam) Compton backscattering. In this Chapter, the beam-beam scattering theory is discussed . First, an analytical formula to estimate the total flux of a Compton X-rays beam (without any collimated condition) is calculated. Then, two approaches to predict the X-ray beam spectral characteristics are adopted: one based upon analytical calculations and the other based upon the CAIN simulation pro- gram. These two approaches have been applied to study the Compton X-ray beam as a function of the real electron beam parameters of electron beam energy spread σ_e and electron beam divergence σ_e'. Analytical formulas to study X-ray flux could be divided into two branches. The first one is the study of X-ray flux without any collimated conditions, the second one is the X-ray flux study in different X-ray beam collimated conditions (energy bandwidth bw and angular acceptance α) where the energy bandwidth is an energy band counting all energies between upper cut-off and lower cut-off energies limit. Finally from the demand of users for specific collimated conditions for ThomX X-ray beam, a high X-ray flux is obtained at a certain value of the electron beam parameters (σ_e' and x_e).

4.1 Expected ThomX Flux from Analytical Cal- culations

4.1.1 Total X-ray flux without collimated conditions

In the ThomX project, an X-ray flux of about $10^{11} - 10^{13}$ ph/sec [4,5] is expected to be achieved. To obtain such a high flux, ThomX is designed to have 1nC electron beam produced by an RF gun with a normalized emittance of less than 10 μrad.

In Compton interactions of two real beams, the total number of X-ray photons produced per second [2, 8], without any selection of the energy bandwidth nor opening angle, is given by the formula:

$$F(\theta_c) = \frac{\Sigma_{th} n_e n_L f_{rep}}{2\pi\sqrt{[(x_e^2 + x_L^2) + \tan^2(\theta_c/2)(z_e^2 + z_L^2)](y_e^2 + y_L^2)^{1/2}}} \quad (4.1)$$

where:

- Σ_{th} is Thomson cross section, $\Sigma_{th} = 6.65\times10^{-29}$ m^2.
- n_e is the number of electrons per bunch.

- n_L is the number of photons per laser pulse.

- f_{rep} is the repetition frequency of the electron beam and laser pulse interaction.

- θ_c is the incident angle of the laser pulse with respect to the electron beam direction.

- x_e, x_L, y_e, y_L, z_e and z_L are the three dimensional bunch sizes of the (Gaussian) electron bunches (index e) and (Gaussian) laser photon pulses (index L).

To obtain high fluxes from Equation 4.1, both the electron bunch and the laser pulse must be focused on a small spot size (small x_e, x_L, y_e, y_L, z_e and z_L) to produce a large number of backscattered X-rays, because of small Thomson cross section. Table 4.1 summarizes the ThomX parameters of the real electron beam and real laser pulse.

Table 4.1: Nominal values of the ThomX parameters [1, 2, 4]

Electron beam energy	50 MeV
Electron bunch charge	1nC
Normalized emittance	10 μm.rad
Transverse size of the electron beam (x_e)	70 μm
Electron bunch length (z_e)	4.80 mm
Laser energy pulse	30 mJ
Transverse size of the laser pulse (x_L)	40 μm
Laser pulse length (z_L)	3 mm
Incident angle (θ_c)	0°

With these proper parameters: the number of electrons in a 1nC bunch is equal to 0.625×10^{10} electrons, since $n_e = \frac{charge\ of\ the\ electron\ bunch}{charge\ of\ the\ electron}$, the number of photons per pulse is equal to 1.6×10^{17} photons for a 1060 nm laser photon with 30 mJ pulse energy [4], $n_L = \frac{laser\ pulse\ energy}{a\ laser\ photon\ enrgy}$, and the repetition frequency is 17.8 MHz, since $f_{rep} = \frac{c}{circumference\ of\ the\ ring\ (16.8m)}$ =17.8 MHz, where c is the speed of light in m/s, the total flux calculated from Equation 4.1 is equal to 2.89 × 1013 ph/sec which is as expected [4, 5].

4.1.1.1 Total Flux dependence on the electron, laser beam transverse sizes and incident angle

One of the main parameters that determine the efficiency of the X-ray production are the beam sizes at the interaction point. Equation 4.1 shows that to increase X-ray flux, the beam size should be as small as possible. The dependence is inversely proportional to the square of the beam size.

To implement the optimization of the photon scattered flux, the programming language MATLAB was chosen. The scattered photons flux is calculated as a function of the transverse size x_e as shown in Figure 4.1. For ThomX the nominal electron beam transverse size x_e is around 70 µm [1].

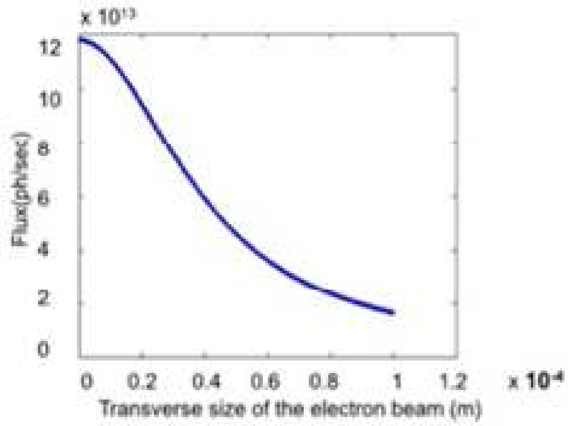

Figure 4.1: The total X-rays flux as a function of electron r.m.s transverse size x_e with constant laser beam waist size x_L of 40 µm.

The obtained variation depicted in Figure 4.1 shows that a decrease of the laser pulse transverse size from 100 to 10 µm increases the flux just by a factor of three (Figure 4.2). The nominal designed value for laser beam transverse size used in ThomX is 40µm [1].

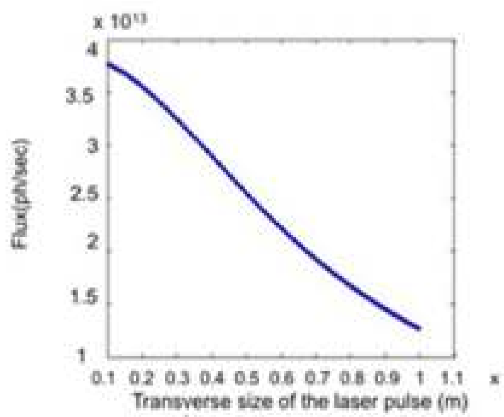

Figure 4.2: The total X-rays flux as a function of the r.m.s laser beam transverse size x_L, for an electron beam of constant transverse size x_e=70 µm.

From Equation 4.1, it is obvious that the maximum flux is obtained when the incident angle θc is zero. Figure 4.3 shows the backscattering X-ray flux as a function of the incident angle θ_c in rad.

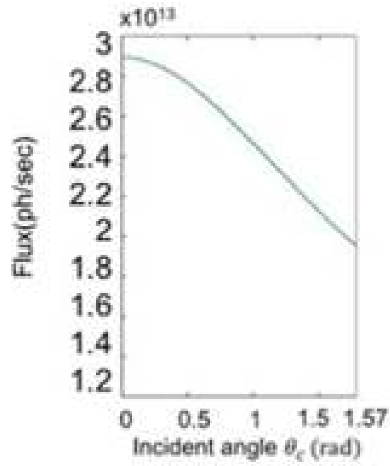

Figure 4.3: The obtained X-ray flux dependence on the incident angle between the laser pulse and the electron beam ($0 \leq \theta_c \leq \pi/2$).

4.1.2 X-ray flux with collimated conditions

4.1.2.1 X-ray flux for selected energy bandwidth

To study the X-ray flux for selected energy bandwidth, the electron beam divergence σ_e' is not taken into account.

Suppose an electron with nominal energy E_0 interacts with a laser photon.

It will then produce an X-ray photon with nominal energy E_{x0}. And if an electron has higher energy E_1, the energy of the produced X-ray photon by this electron at the same scattering angle Ex1 will be greater than E_{x0}. So, the X-ray flux in a given energy bandwidth centered around the nominal X-ray energy E_{x0} will decease as the energy spread of the electron beam increases since the diaphragm only selects the central part of the beam (i.e. its higher energy part). The flux in the given bandwidth ΔE centered around the on-axis X-ray energy is [2]:

$$F_{bw}(\sigma_e) = \frac{3}{2}F(\theta_c)bw\left\{1-(bw-bw^2/2)ERF\left[bw/(2\sqrt{2}\sigma_e)\right] - 6\sqrt{2/\pi}\sigma_e\exp(-bw^2/8\sigma_e{}^2)\right\} \tag{4.2}$$

where:

- F (θ_c) is the total flux as expressed and calculated in Section 3.1.1.
- bw is the chosen relative energy bandwidth of the X-ray photons.
- ERF is the error function.

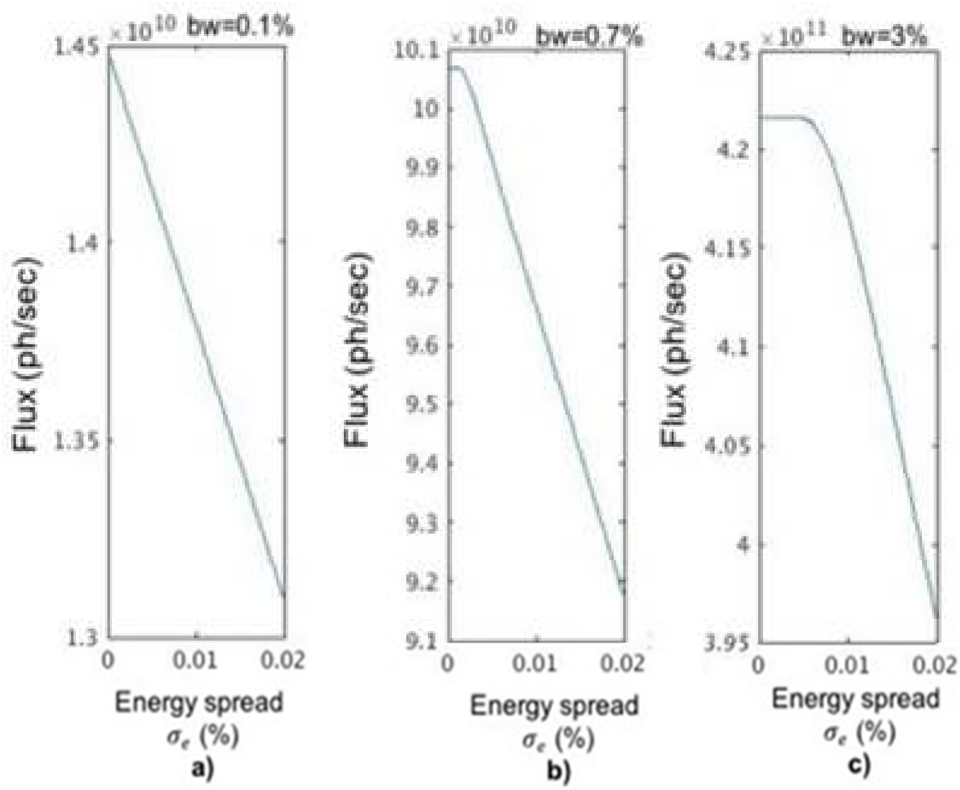

Figure 4.4: The X-ray flux as a function of energy spread for different energy bandwidths. a) bw=0.1%, b) bw=0.7%, c) bw=3%.

Figure 4.4 shows the relation of the flux as a function of the electron relative energy spread for different energy bandwidths. It can be noticed that for a small energy bandwidth (bw=0.1%), the energy spread of the electron beam affects and leads to a decrease of the flux even for a small electron beam energy spread σ_e.

4.1.2.2 X-ray flux for selected angular acceptance

As already discussed in the previous section, an X-ray photon of a given energy is scattered with a specific angle. In case of perfect laser and electron beams, the scattering angle has a univocal relation with the energy of the X-ray. The angular acceptance is the selection of the emission angle of the X-ray with respect to z-axis. But with real electron beam with natural divergence, the flux for a given angular acceptance (opening angle) decreases as the electron beam divergence increases. The effect of the electron beam energy spread is negligible (σ_e=0) [2].

The flux F_α in a given angular acceptance α as a function of electron beam divergence σ_e' is given by [2]:

$$F_\alpha(\sigma_e') = \frac{3}{2} F(\theta_c) \frac{\mu_\alpha}{(1+\mu_\alpha/2)^4} \left[1 + \frac{(\mu_\alpha)^2}{4} - 4\gamma^2 \sigma_e'^2 \left(\frac{2 - \frac{\mu_\alpha}{2} + \mu_\alpha{}^2/4}{1 + \frac{\mu_\alpha}{2}} \right) \right] \tag{4.3}$$

where:

- F_α is the flux in a given angular acceptance.

- α is the angular acceptance around the z-axis.

- $\mu_\alpha = \gamma^2 \alpha^2$.

- F (θ_c) is the total flux calculated in Section 3.1.1.

For ThomX with a 50 MeV electron beam, Equation 4.3 is valid as long as $\mu_\alpha \leq 0.15$ and $\gamma^2 \sigma_e'^2 \leq 0.03$ [2].

Figure 4.5 displays the obtained flux as a function of electron beam divergence for different values of the angular acceptance α and calculated with parameters of Table 4.1 keeping the electron beam emittance value variable. For the selected opening angles (α =1mrad, α =2mrad), the obtained flux decreases as electron divergence increases.

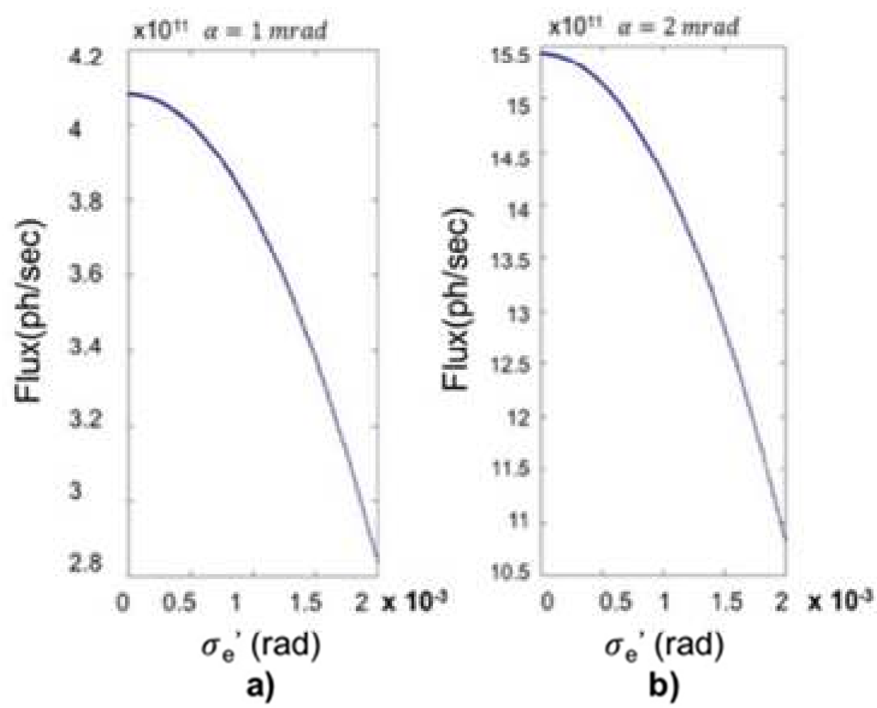

Figure 4.5: X-ray flux as a function of electron beam divergence σ_e' for two different values of the angular acceptance α . a) α =1mrad, b) α =2mrad.

4.1.2.3 X-ray flux for a selected angular acceptance and energy bandwidth dependence on the electron beam divergence

In this section, the electron beam energy spread is ignored (σ_e=0) and the X-ray flux in a given angular acceptance and in a given energy bandwidth, as given in Equation 4.4 is calculated. First, we will convert the energy bandwidth into the angle θ_{bw}, where $\theta_{bw} = \frac{\sqrt{bw}}{\gamma}$ [2]. The energy bandwidth becomes equivalent to an angular acceptance which defines a cone whose axis is along the direction of the electron beam and whose half opening is θ_{bw}. For instance, with the ThomX parameters when the bandwidth is 0.1%, it corresponds to a θ_{bw} of 0.316 mrad. The flux of the scattered X-ray within the angular acceptance α and within the given energy bandwidth bw is given by the following formula [2]:

$$F_{\alpha,bw}(\sigma_e') = \frac{F(\theta_c)}{\theta_{bw}^2}\left[\theta_m^2 + \sigma_e'^2\left\{\exp\left[-\frac{(\alpha-\theta_{bw})^2}{2\sigma_e'^2}\right] - \exp\left[-\frac{(\alpha+\theta_{bw})^2}{2\sigma_e'^2}\right]\right\} + \sqrt{\frac{\pi}{2}}\sigma_e'\theta_M ERF\left(\frac{\theta_M-\theta_m}{\sqrt{2}\sigma_e'}\right) + \sqrt{\frac{\pi}{2}}\sigma_e'\theta_m ERF\left(\frac{\theta_M}{\sqrt{2}\sigma_e'}\right) - \sqrt{\frac{\pi}{2}}\sigma_e'(\theta_{bw}+\alpha) ERF\left(\frac{\alpha+\theta_{bw}}{\sqrt{2}\sigma_e'}\right)\right] \tag{4.4}$$

Where F (θ_c) is the total flux calculated in Section 3.1.1, θ_m equals the minimum value between α and θ_{bw}, θ_M equals the maximum value between α and θ_{bw} and ERF is the error function.

Figure 4.6 represents the obtained dependence between the X-ray flux and the electron beam divergence for different values of the bandwidth and the angular acceptance, and for the ThomX parameters of Table 4.1 except the electron beam emittance value which is variable.

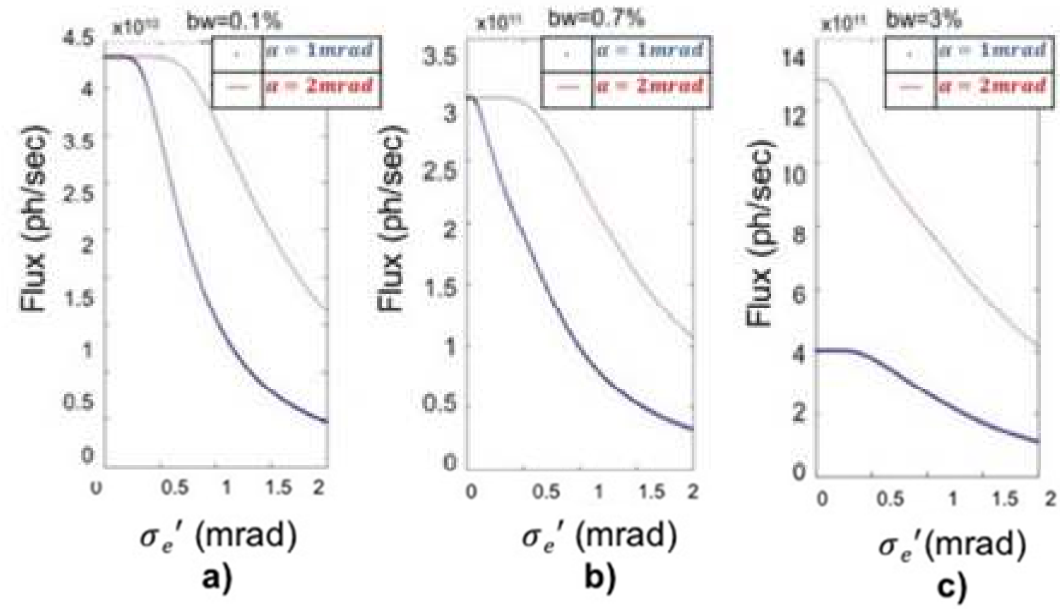

Figure 4.6: X-ray flux as a function of the electron beam divergence σ_e' in a given angular acceptance α and a given bandwidth bw. a) bw=0.1%, b) bw=0.7%, c) bw=3% (red line α =2 mrad and blue line α =1mrad).

4.1.2.4 X-ray flux for a selected angular acceptance and energy bandwidth dependence on the electron beam energy spread

The electron beam divergence is now ignored ($\sigma_e'= 0$), and we calculate here the X-ray flux in a given angular acceptance α and a given energy bandwidth bw by taking only the electron beam energy spread σ_e into account [2]. The expression of the flux is:

$$F_{\alpha,bw}(\sigma_e) = \frac{F(\theta_c)}{2bw}\left\{\sqrt{\frac{8}{\pi}}\sigma_e\left[\exp\left(-\frac{(\mu_\alpha+bw)^2}{8\sigma_e{}^2}\right)-\exp\left(-\frac{(\mu_\alpha-bw)^2}{8\sigma_e{}^2}\right)\right]\right.$$
$$\left.+(\mu_\alpha+bw)ERF\left(\frac{\mu_\alpha+bw}{2\sqrt{2}\sigma_e}\right)-(\mu_\alpha-bw)ERF\left(\frac{\mu_\alpha-bw}{2\sqrt{2}\sigma_e}\right)\right\} \tag{4.5}$$

where:

- $\mu_\alpha = \gamma^2 \alpha^2$.
- F (θ_c) is the total flux expressed in Section 3.1.1
- ERF is the error function

Figure 4.7 shows the obtained variation of the X-ray flux as a function of the electron beam energy spread for different selected angular acceptance and bandwidth values and for the ThomX parameters of Table 4.1.

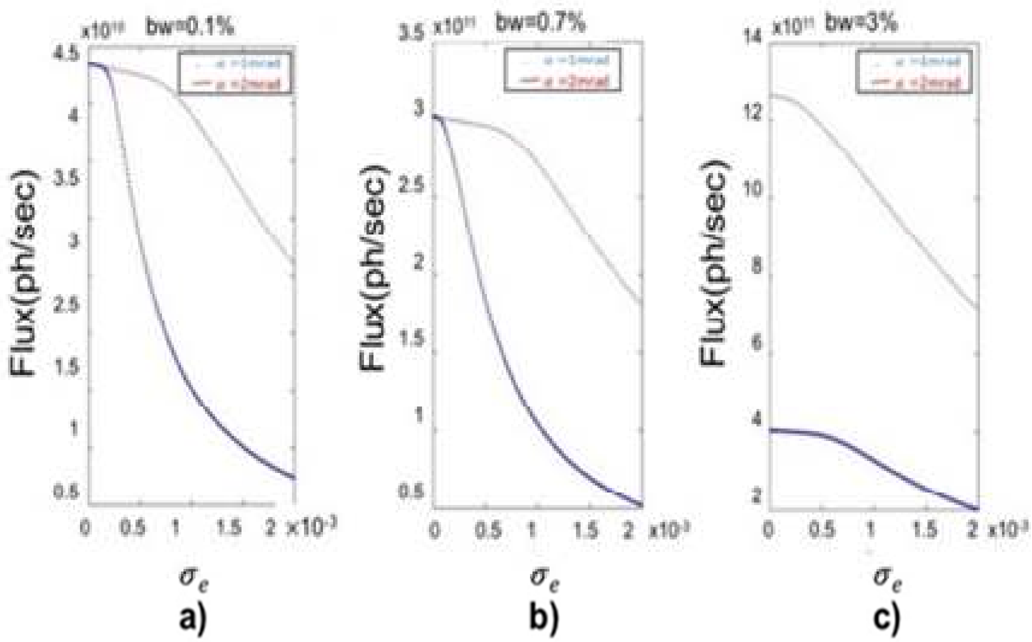

Figure 4.7: The X-ray flux as a function of the electron beam energy spread σ_e in a given angular acceptance α and a given bandwidth bw. a) bw=0.1%, b) bw=0.7%, c) bw=3% (red line α =2 mrad and blue line α =1mrad).

4.1.2.5 X-ray flux for a selected angular acceptance and energy bandwidth dependence on both the electron energy spread and the electron divergence

Here, we take both the electron beam energy spread σ_e and the electron beam divergence σe0 into account to calculate the X-ray flux. When the energy spread σ_e of the electron beam is dominant with respect to the electron beam divergence σ_e', we can use the same flux as Formula 4.5, but with a small correction to take into account the electron beam divergence.

For this, the energy bandwidth in terms of θ_{bw} angle has to be modified as $bw_{modified} = \sqrt{bw^2 + (2\sigma_e)^2}$ [2]. However, when the electron beam divergence plays a dominant role with respect to the energy spread, we will get the same flux as Formula 4.4, but with a small correction to take into account the electron beam energy spread σ_e. The modified energy spread to take the electron beam divergence into account is $\sigma_{e(modified)} = \sigma_e + \gamma^2\sigma_e'^2$ [2].

Figure 4.8 shows the obtained X-ray flux as function of the electron beam divergence for different values of the angular acceptance and the energy band- width and taking into account the electron beam energy spread (σ_e= 0.5% and 1.5%). Calculations have been performed with the ThomX parameters of Table 4.1 except the variable electron beam normalized emittance value.

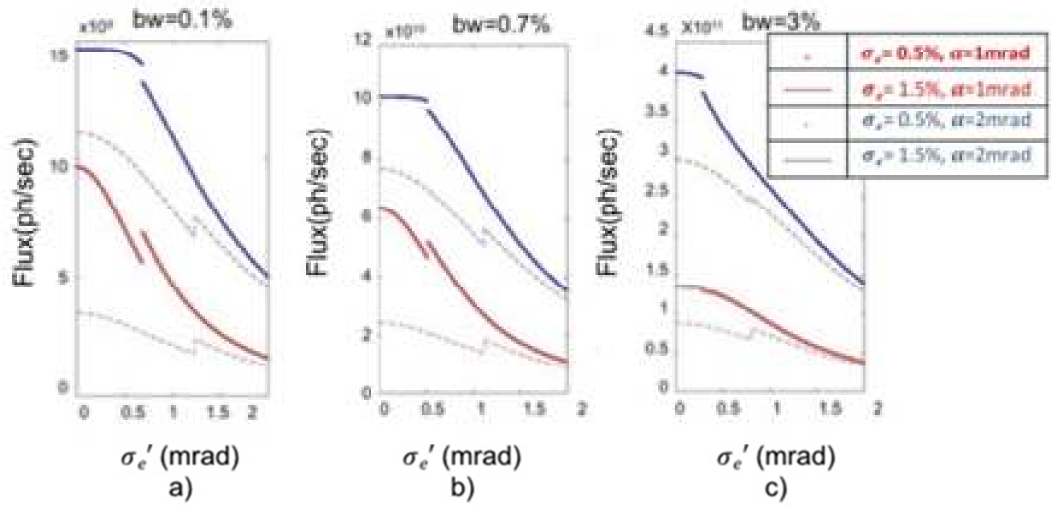

Figure 4.8: The flux as a function of the electron beam divergence σ_e' for an electron energy spread of 0.5% and 1.5% and for an angular acceptance of 1 mrad and 2 mad, for different bandwidth values. a) bw=0.1%, b) bw=0.7%, c) bw=3%. The red line is for α =1mrad, the blue line is for α =2 mrad, the dotted line is for σ_e=0.5% and the dashed line is for σ_e=1.5%.

These discontinuities shown in the curves of the Figure 4.8 are due to the use of Equations 4.4 and 4.5 with the previously discussed corrections. When $2\gamma^2\sigma_e'^2$+ bw$\leq \sqrt{bw^2 + (2\sigma_e)^2}$, Equation 4.5 should be used by replacing σ_e by $\sigma_e+\gamma^2\sigma_e'^2$. Otherwise Equation 4.4 is used where bw is replaced by$\sqrt{bw^2 + (2\sigma_e)^2}$.

4.1.3 Optimization of the machine operating point

Increasing the divergence of the electron beam causes the X-ray flux to decrease for a selected energy bandwidth and angular acceptance. From Equation 4.1 when the transverse size of the electron x_e decreases the flux will increase. The electron beam normalized emittance $\varepsilon_N = \gamma\ \sigma_e' x_e$, the electron beam transverse size varies as the electron beam divergence changes since both the normalized emittance and gamma are constants.

Because of constant normalized emittance, as the electron beam divergence σ_e' increases its transverse size x_e decreases.

Figure 4.9 represents the X-ray flux in 0.2 mrad angular acceptance and 1×10^{-4} energy bandwidth as a function of electron beam divergence σ_e' for a constant normalized emittance of 10µm.rad. As mentioned before, from Equation 4.1, a decrease in the electron beam transverse size x_e leads to an increase in the X-ray flux. So at a specific value of the electron beam transverse size (certain value of electron beam divergence) we get a maximum flux. The maximum flux corresponding to specific value of the electron beam divergence σ_e' is found to be equal to 0.8 µrad (which will be used later in my simulations).

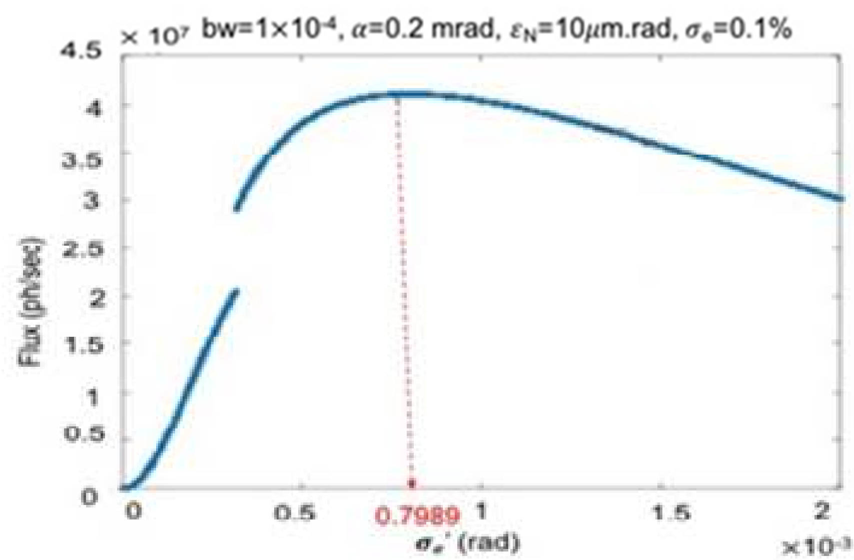

Figure 4.9: X-ray flux a given angular acceptance α of 0.2 mrad and an energy bandwidth of 0.01% as a function of σ_e', for σ_e = 0.1%, ε_N =10µm.rad. The maximum flux of 4.018×10^7 ph/sec is obtained when σ_e' is equal to 0.8 mrad which corresponds to x_e equal 125 µm.

4.2 Expected ThomX X-ray Beam from the CAIN Simulation Program

4.2.1 The CAIN program

In this section the CAIN program [18, 19] will be used. CAIN is based on a Monte-Carlo code for interactions involving high energy particles (electrons, positrons and photons). CAIN provides the ability to simulate Compton scattering and to study the resulting effect on the flux of the backscattered photons. The CAIN simulation program is written by K. Yokoya et al. [18], it uses a dedicated, elaborate meta-language for defining the input parameters.

The CAIN program simulate interactions between a laser pulse and an electron beam. Here, we use this program with the ThomX nominal beam parameters of Table 4.1. The goal is to study the effect of the beams parameters on the backscattered X-ray spectrum.

In the ThomX ring, the charge of the electron bunch is 1nC. This corresponds to a huge number of electrons, about 10^{10} electrons in a single bunch, this requires a very long computational time in order to simulate each electron individually. In order to reduce the computational time and render the technique more tractable, the electrons are divided into groups called macro-particles. For instance a 1 nC electron bunch contains 0.625×10^{10} electrons and are divided into several macro-particles each macro-particle containing a certain number of electrons. In our simulation, we use

10^7 macro-particles and each macro-particle contains 10^3 electrons. Doing such simulations takes more than eight hours per simulation.

Also, the electron-laser collision time is divided into 400 time steps. At each time step, the Compton scattering process between an electron macro- particle and a laser photon macro-particle is simulated and produce a backscattered photon macro-particle according to the cross section of Compton process. At the end of the simulation, the output files are containing all input and output particles' information.

By using the CAIN program, we intend to investigate the effects of the electron beam energy spread σ_e and the electron beam divergence σ_e' on the spectral and angular Compton X-rays flux.

4.2.2 Simulations and results

It is also possible to see the effect of the electron beam parameters on the total flux. For this, simulations were performed in which some parameters were changed in order to study how they affect the flux and the energy distribution of the scattered photons.

The first CAIN simulation was performed with the following input parameters:

- ε_N =1μm.rad.
- σ_e= 0.1%.
- σ_e'=80μrad.
- x_e =125 μm.

Figure 4.10 shows the angle and energy dependence of the X-rays flux resulting from this simulation. The maximum value of the X-ray flux for on-axis X-rays in a given $\Delta\theta_x$ is 2.66×10^{10}ph/sec, appendix A gives the details of the calculation of this flux. This energy broadening of the X-ray spectrum is due to the electron beam energy spread and the divergence of the electron beam. The spectral distribution of X-ray macro-particles as a function of their energy is presented in Figure 4.11. Figure 4.12 displays the detailed of Figure 4.11 distribution of the X-ray photon energy spectrum near the Compton edge.

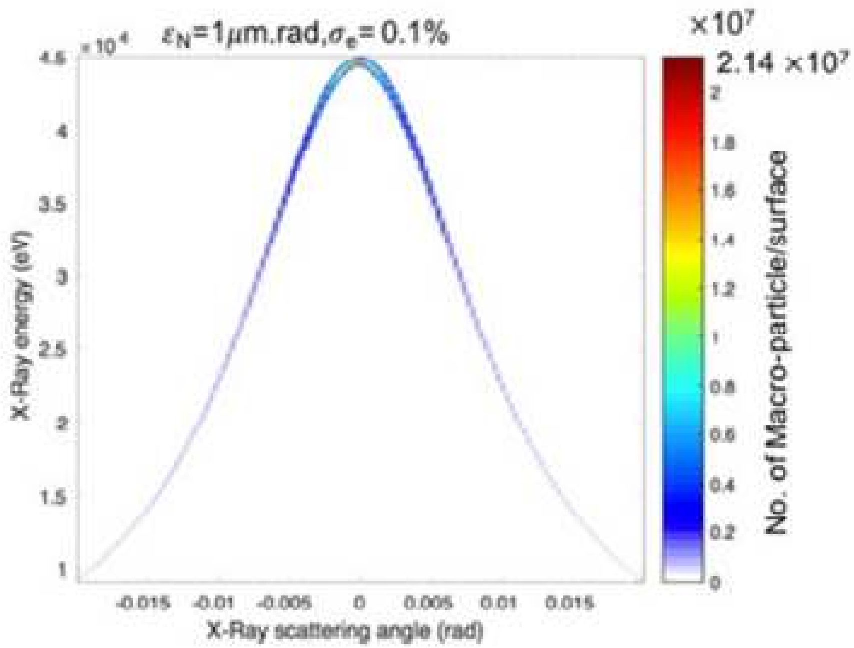

Figure 4.10: Angle and energy dependence of the spectral flux (color code) which indicates the surface density of the photon macro-particles (from white as less intense to red as more intense) resulting from CAIN simulation performed with the following electron beam parameters: ε_N =1μrad.m, σ_e' =80μrad and σ_e=0.1%. The number of bins for the θ_x-axis were 133 bin where $\Delta\theta_x$=0.3mrad and for the E_x-axis were 159 bins where E_x=0.5%. The maximum number of on-axis macro-particle/surface is 2.14×10^7.

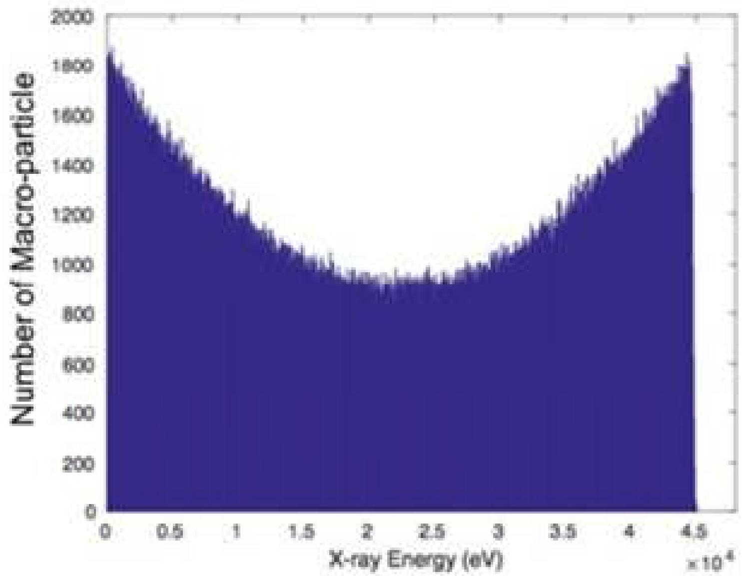

Figure 4.11: Spectral distribution of the Compton photons resulting from a CAIN simulation performed with the following electron beam parameter: σ_e = 0.1%, ε_N = 1 µm.rad and σ_e' =80µrad. For the E_x-axis the number of bins used were 1000 bin, ΔE_x=0.1%.

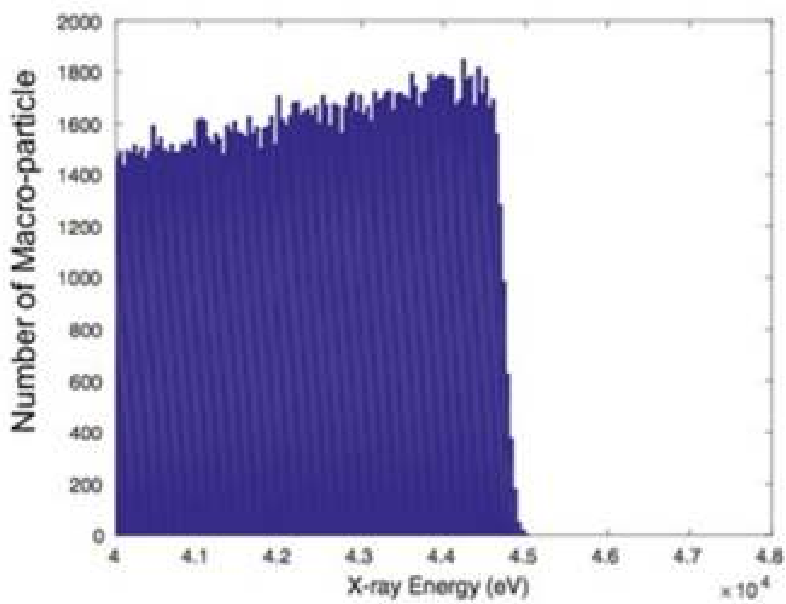

Figure 4.12: As Figure 4.11, where the Compton edge is highlighted. The maximum energy of X-rays obtained is 45.031 keV.

As expected, because of the good quality of the electron beam used in the simulation (ε_N = 1 μm.rad, σ_e'=80μrad and σ_e = 0.1%), the spectral and the angular flux of Figure 4.10 remains narrow, i.e. quite close to the energy-angle curve resulting from interactions between two ideal incident beams (Figure 2.2). For the same reason, the Compton edge tail in Figure 4.12 due to the small energy spread σ_e is almost invisible. This distribution is near the perfect one shown in Figure 2.4.

To evaluate the influence of the electron beam divergence, a second simulation is performed with electron beam parameters of the normalised emittance ε_N = 10μ rad.m and the divergence σ_e' = 800μrad (the other parameter σ_e is remaining the same). The result is shown in Figure 4.13. In comparison with Figure 4.10, the effect of the electron beam divergence generates a horizontal broadening; X-ray photons with the same energy have now different scattering angles. The main consequence is a decreasing of the number of mono-energetic photons observed at a given angle.

The maximum obtained value of the on-axis X-ray flux in a given $\Delta\theta_x$ is 8.831×10^9ph/sec, appendix A gives the details of the calculation of this flux.

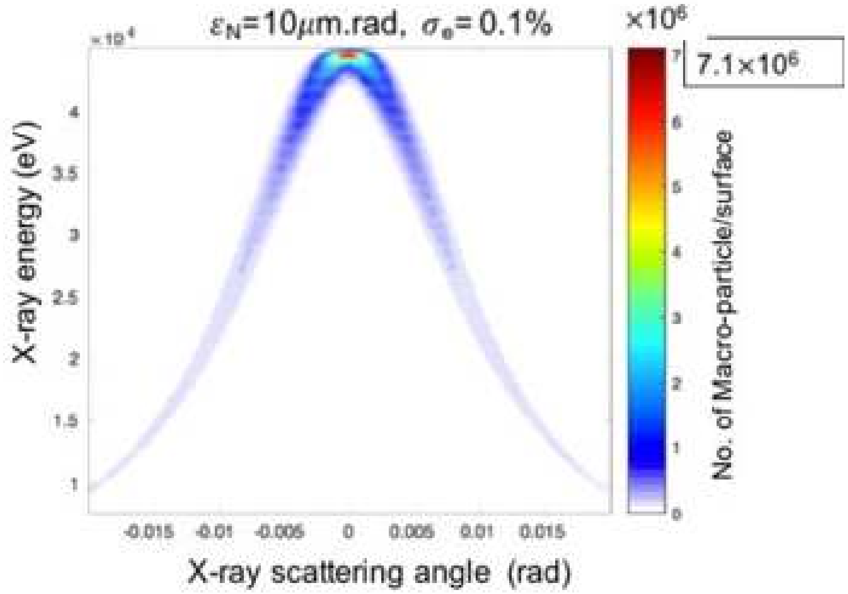

Figure 4.13: Angle and energy dependence of the spectral flux (color code) which indicates the surface density of the photon macro-particles (from white as less intense to red as more intense) resulting from CAIN simulation performed with the following electron beam parameters: ε_N =10μrad.m, σ_e' =800μrad and σ_e=0.1%. The number of bins for the θx-axis were 133 bin where $\Delta\theta_x$=0.3 mrad and for the E_x-axis were 159 bins where ΔE_x=0.5%. The maximum number of on-axis macro-particle/surface is 7.1×10^6.

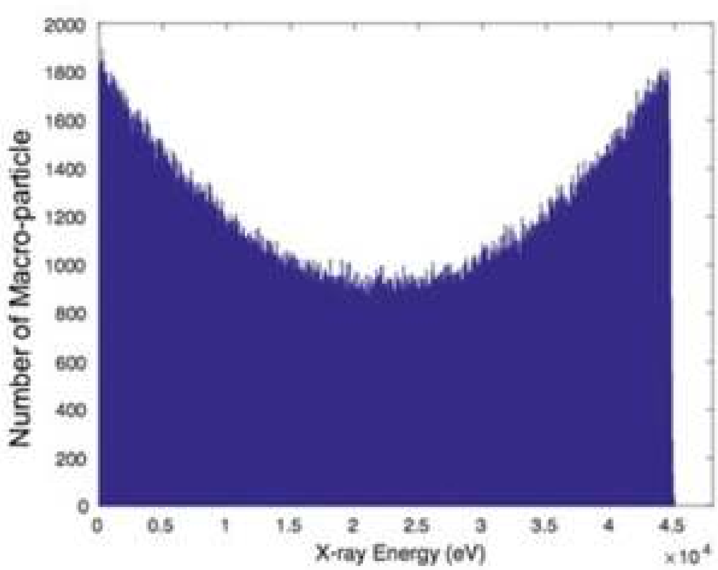

Figure 4.14: Spectral distribution of the Compton photons resulting from a CAIN simulation performed with the following electron beam parameter: σ_e = 0.1%, ε_N = 10μm.rad and σ_e' =800μrad. For the E_x-axis the number of bins used were 1000 bin, ΔE_x=0.1%.

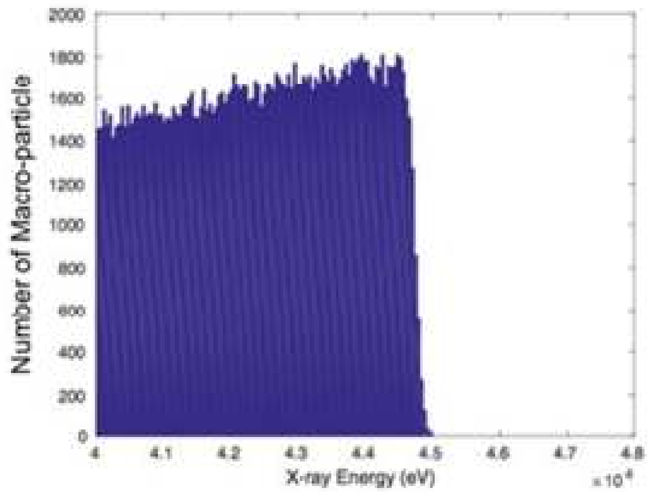

Figure 4.15: As Figure 4.14, where the Compton edge is highlighted. The maximum energy of X-rays obtained is 44.999 keV.

As expected, the spectral distribution shown in Figure 4.14 and 4.15 has the same shape of those in Figure 4.11 and 4.12 since the value of the energy spread σ_e used in the CAIN simulations is unchanged (σ_e=0.1%).

Finally, to evaluate the effect of the electron beam energy spread σ_e on the X-ray spectrum, we performed a third simulation where the electron energy spread σ_e is increased. The electron beam parameters' values used in the CAIN simulation are as the following:

- ε_N =1µrad.m
- σ_e'=80µrad
- x_e= 125 µm
- σ_e=1% (larger value than the value was used Figure 4.10 and 4.13)

The angle and energy dependence of the X-ray flux is shown in Figure

4.16. The maximum obtained value of the on-axis X-ray flux in a given $\Delta\theta_x$ is 4.17×10^9ph/sec, appendix A gives the details of the calculation of this flux.By comparing Figure 4.16 with Figure 4.10, the effect of the electron beam energy spread can be visualized as a larger energy broadening (i.e. a "vertical" broadening); the X-ray photons with the same scattering angle have different energies.

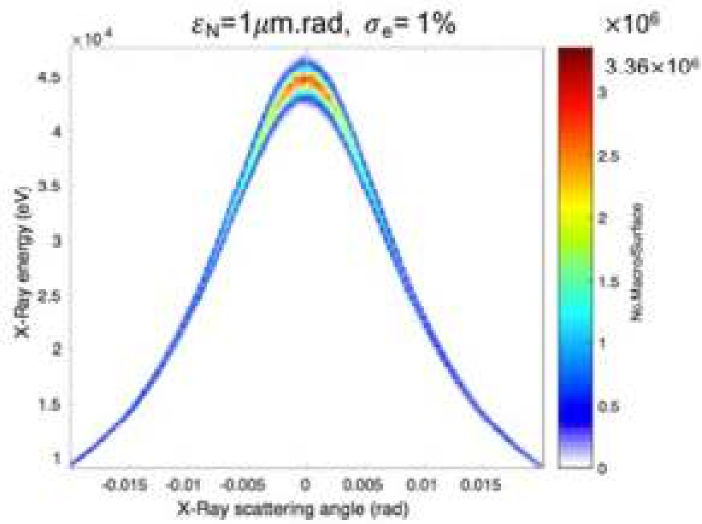

Figure 4.16: Angle and energy dependence of the spectral flux (color code) which indicates the surface density of the photon macro-particles (from white as less intense to red as more intense) resulting from CAIN simulation performed with the following electron beam parameters: ε_N =1µrad.m, σ_e' =80µrad and σ_e=1%. The number of bins for the θ_x-axis were 133 bin where $\Delta\theta_x$=0.3mrad and for the Ex-axis were 159 bins where ΔE_x=0.5%. The maximum number of on-axis macro-particle/surface is 3.36×10^6.

The effect of the energy spread (σ_e) is more highlighted on the X-ray spectral distribution shown in Figures 4.17 and 4.18. Indeed we see clearly in Figure 4.18 that a tail appeared at the Compton edge energy. The main effect of the electron energy spread is to degrade the X-ray beam monochromaticity at a given observation angle.

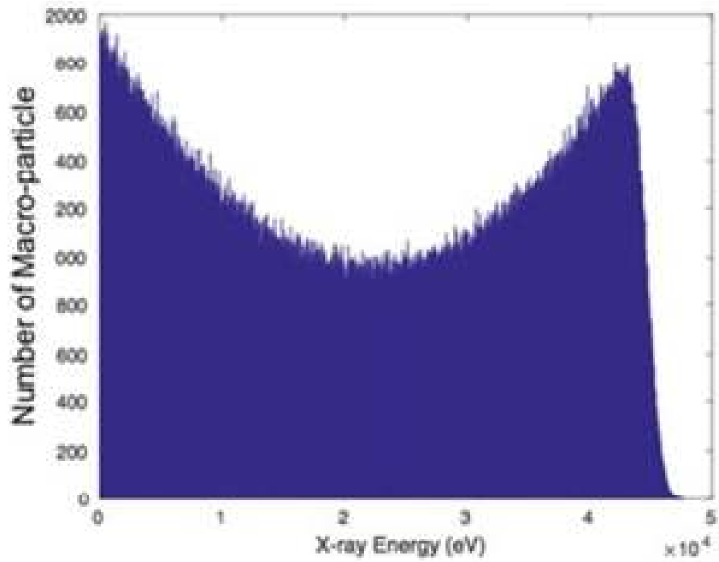

Figure 4. 17: Spectral distribution of the Compton photons resulting from a CAIN simulation performed with the following electron beam parameter: σ_e = 1%, ε_N = 1μm.rad and σ_e' =80μrad. For the E_x-axis the number of bins used were 1000 bin, ΔE_x=0.1%

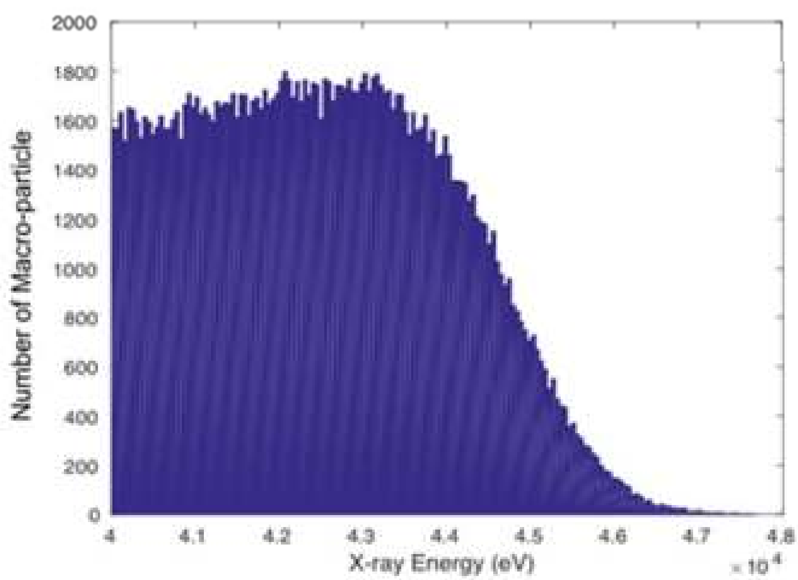

Figure 4.18: As Figure 4.17, where the Compton edge is highlighted. The maximum energy of X-rays obtained is 47.67 keV.

Chapter Five

Results of Flux Estimation within a CdTe Detector

5.1 Introduction

In the ThomX experiment, in order to measure the spectral flux of the scattered X-ray photons, a cadmium telluride (CdTe) detector will be used. This detector has a 3mm × 3mm square surface. The detector will be placed on the trajectory of the beam at a fixed distance r from the interaction point. The detector position makes an angle θ with respect to the z-axis and φ with respect to the x-axis as shown in Figure 5.1.

The detector finite area is denoted by A_D. The X-ray photons reaching the detector have an angular spread of dθ , which depends on how far the detector is located from the interaction point (r). The acceptance angle of the finite- area detector decreases as the detector distance increases from the interaction point. It also has an azimuthal spread of dφ, where dθ and dφ are determined by the fixed detector width (W) and are the angular intervals subtended by the detector of fixed width W.

The number of Compton X-ray photons per unit time that enters a detector (which has a specific area) is estimated through two different methods. The first one consists on using analytical formulas to determine the spectral and spatial flux of Compton X-rays. From Equation 4.3 the photons flux at given angular acceptance (for a given value of θ and φ varies from 0 to 2π) can be calculated. The Second method, the CAIN program is used (with the same electron beam parameters that is used in analytical formulas) to calculate the number of Compton X-rays per (with some constrains on the polar angle $\theta \leq 3.8$ mrad [2]). Both results from these two different methods will be compared. Finally, by changing the detector position as shown in Figure 5.2, the number of photons that enter the detector per unit time will be calculated.

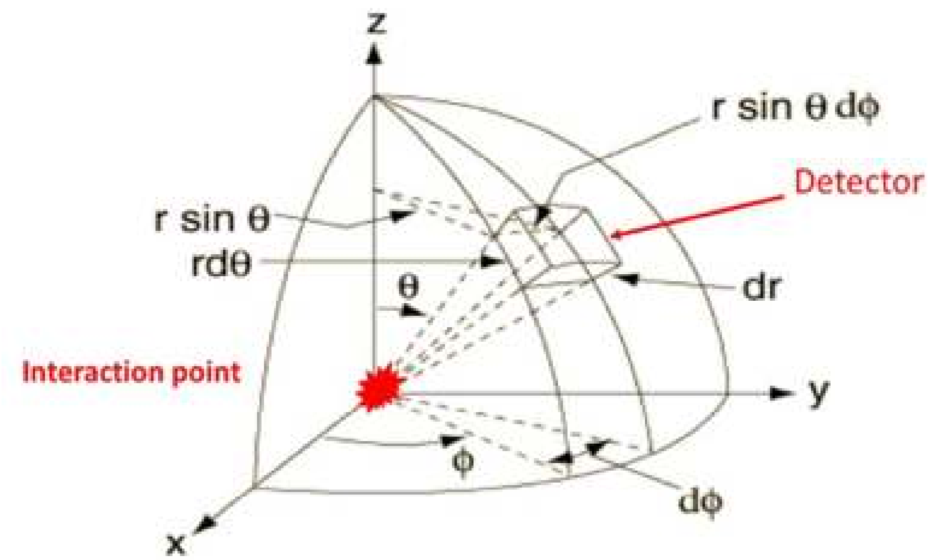

Figure 5.1: The detector position in term of polar angle θ, azimuthal angle φ and radial distance r [20].

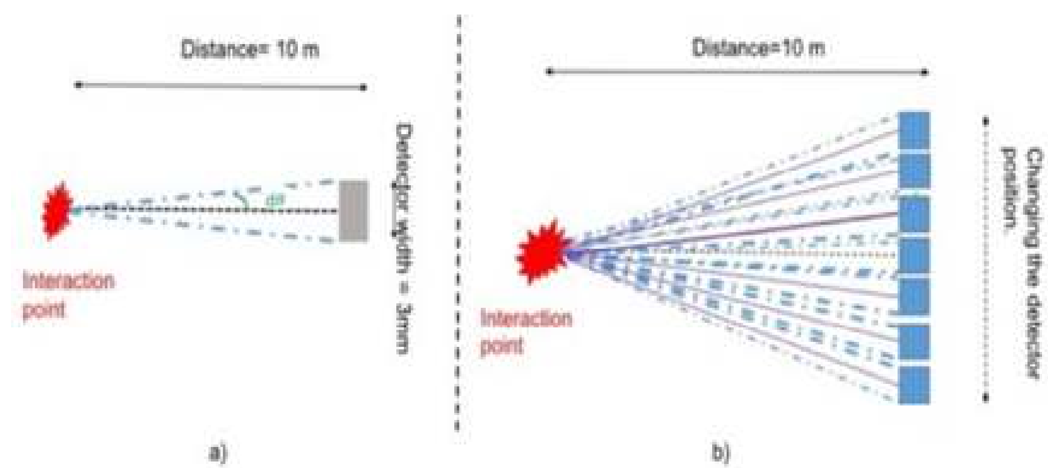

Figure 5.2: a) The detector is located on the symmetric axis. b) Changing the detector position as a function of elevation point from the symmetric axis.

5.2 Theoretical Method

The photon flux is calculated at a position of the detector which is given by spherical coordinate components (r, θ, φ). Equation 4.3 allows us to calculate the photon flux in a given angular acceptance. In Figure 5.3, the desired flux inside the annular ring (grey area) is determined by measuring the flux subtended by the two acceptance angles admitting flux which are (θ + dθ) and (θ - dθ) and calculating the difference between them. The received flux in this area (F_R) yields a contribution to the flux received by a detector which has the same area of the annular ring (A_R). The flux which is measured by the detector with specific A_D, is denoted F_D which is approximated by:

$$F_D \cong F_R \times \left(\frac{A_D}{A_R}\right) \tag{5.1}$$

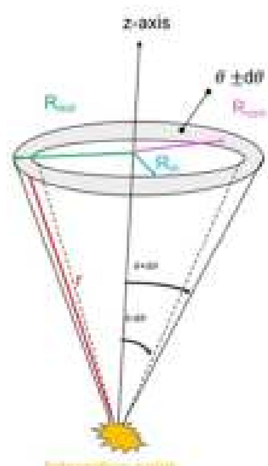

Figure 5.3: Scheme of the surface of the ring located at a distance r from the interaction point and defined by the polar angle θ - dθ and θ + dθ. The desired flux (F_R) is determined by calculating the flux subtended by the two acceptance angles, flux for a given θ+ dθ and flux for a given θ - dθ and calculating the difference.

Example:

- The distance of the detector position from the interaction point r is 10 m (in the ThomX).
- The polar angular acceptance θ is chosen to be equal to θ = 3 mrad (in the ThomX by using a 50MeV electron beam, Equation 4.3 is valid as long as θ ≤ 3.8 mrad).
- the angular spread of dθ is $\frac{w/2}{r}$.
- The electron beam divergence σ_e' is 800μrad, ε_N = 10μm.rad and x_e=125 μm, which are obtained from Figure 4.9.

First, by using Equation 4.3, the flux of the selected acceptance angle of θ + dθ is calculated, then the flux at a smaller acceptance angle of θ − dθ is calculated. If the flux of the smaller acceptance angle (F_S) is subtracted from that corresponding to larger acceptance angle (F_L), then the flux inside the annular ring will be obtained F_R (Figure 5.3).

The difference between the flux in the larger opening angle (i.e. $\alpha_+ = \theta + d\theta$), $F_L = F_{\alpha+} (\sigma_e')$ and the flux of the smaller opening angle (i.e. $\alpha_- = \theta - d\theta$), $F_S = F_{\alpha-} (\sigma_e')$ is the flux inside the annular ring.

$$\begin{aligned} F_R &= F_L - F_S \\ &= \left(F_{\alpha_+}(\sigma_e') - F_{\alpha_-}(\sigma_e') \right) \end{aligned} \tag{5.2}$$

The area of the ring is given by:

$$A_R = \pi({R_{out}}^2 - {R_{in}}^2) \tag{5.3}$$

where:

$$R_{out} = r\ \sin(\theta + d\theta) \tag{5.4a}$$

$$R_{in} = r\ \sin(\theta - d\theta) \tag{5.4b}$$

$$R_{Cen} = r\sin(\theta) \tag{5.4c}$$

From Equations 5.4 (a, b and c) and 5.3, the area of the annular ring is given by:

$$A_R = \pi r^2\ [\sin^2(\theta + d\theta) - \sin^2(\theta - d\theta)] \tag{5.5}$$

From Equation 4.3 the flux in a larger given opening angle $F_L = F_{\alpha+}\ (\sigma_e')$ and the flux in a smaller opening angle $F_S = F_{\alpha-}\ (\sigma_e')$ can be obtained and by using Equation 5.2, the net flux was obtained. By dividing the ring into small squares of area, where the detector area is $A_D = W^2$, the flux which is measured by the detector is given by:

$$F_D \cong \left(F_{\alpha_+}(\sigma_e') - F_{\alpha_-}(\sigma_e')\right)\left[\frac{W^2}{\pi r^2\left(\sin^2(\theta+d\theta)-\sin^2(\theta-d\theta)\right)}\right] \tag{5.6}$$

With the use of these parameters r=10m, θ =3mrad, W =3mm, σ_e'=800μrad and x_e=125 μm and by using Equations 5.2 and 4.3, the flux of the dark area of the ring can be calculated as follows:

F_R=F_L - F_S =(1.264×10^{12} - 1.08×10^{12}) ph/sec = 1.84×10^{11}ph/sec.

where the detector area (A_D) equals 9×10^{-6} m^2.

From Equation 5.6, the total flux reaching the detector is calculated to be 2.93×10^9 ph/sec; This is the value which is obtained (F_D) for a selected θ =3mrad, r=10m and W =3mm.

5.3 Simulation by Using the CAIN Program for CdTe Detector

We have also calculated the angular and the spectral flux of the X-ray scattering photons by using the CAIN simulation program. For this simulation, we used the following parameters:

- The normalized emittance ε_N of 10μm.rad.
- The electron beam divergence σ_e' equals to 800μrad.
- The electron beam energy spread σ_e of 0.1%.
- The electron bunch length z_e of 10 psec.

The CAIN outputs for each scattered X-ray photon are the X and Y directions, momentum in the x, y and z directions (P_X, P_Y and P_S). From these outputs, we can get the polar angle (θ) and the azimuthal angle (φ) for each photon.

where:

- $\theta = \arctan\left(\frac{\sqrt{P_X{}^2 + P_Y{}^2}}{P_S}\right)$ with $\theta \in [0, \pi]$.
- $d\theta = \frac{W/2}{r}$, where r is the distance from the interaction point we just divide by r to convert the angle into radians.
- $\varphi = \arctan\left(\frac{P_Y}{P_S}\right)$ with $\varphi \in [0, 2\pi]$.

For example, if the polar angle θ was selected to be equal to 3 mrad, and a random value of the azimuthal angle φ was chosen at π /5 (φ varies from 0 to 2π), the CAIN simulation program yields a flux of 3.02×10^9 ph/sec, which is in a good agreement with the value obtained from the analytical expression.

Finally, we have checked that if the polar angle remains constant (θ =3mrad) and the azimuthal angle φ is changing from 0 to 2π ending with a closed circle (Figure 5.4); the flux generated by CAIN, as expected, remains constant (Figure 5.5).

For this, the used parameters are:

- θ = 3 mrad.
- $\Delta\varphi = 0.1$

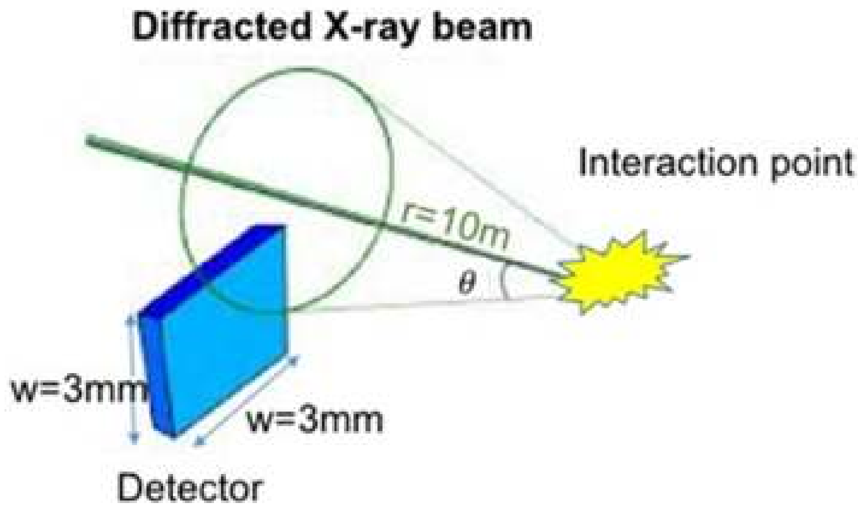

Figure 5.4: Detector located at r =10m from the interaction point with certain polar angle θ and changing the azimuthal angle φ with respect to X-ray maximum energy axis.

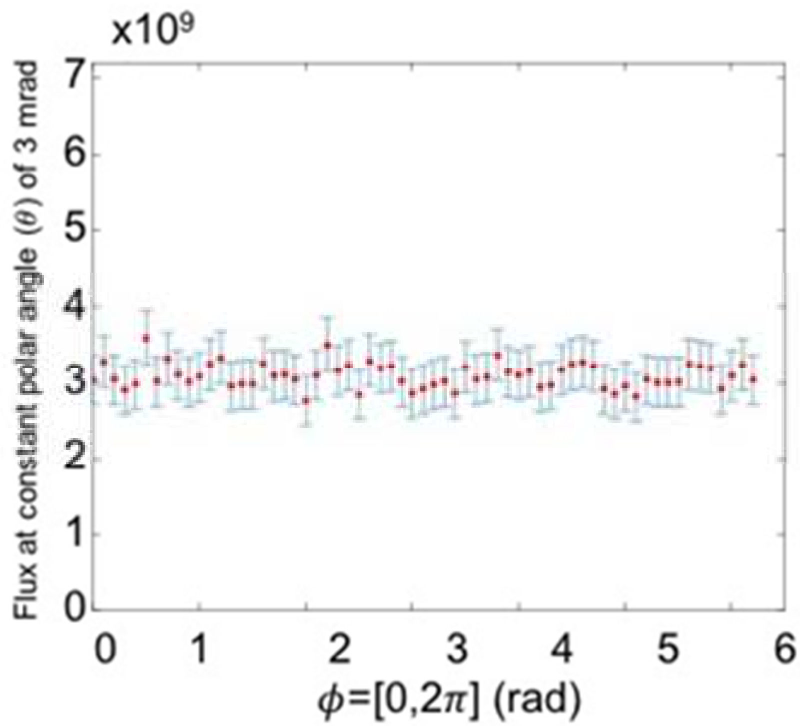

Figure 5.5: By using the CAIN program, the flux of the Compton X-ray of constant polar angle θ =3 mrad and dθ =0.15 mrad as a function of the azimuthal angle changes from 0 to 2π rad which contribute to flux of a ring. The maximum value of the flux is 3.59× 10^9 ph/sec at φ = 0.5 mrad, whereas the minimum value of the flux is 2.76 × 10^9 ph/sec at φ =2 rad.

The distribution of data values is represented by showing a single data point, representing the mean value of data. Error bars (statistical uncertain- ties) are used to quantify uncertainty in graph of statistical metrics. Flux of X-ray photon obeys the Poisson equation of statistical error propagation, for which the error in counting number of photons (N) in 1 second is $\sqrt{N}$ [21]. For example, if 10000 photons are counted in 1 sec, it can be concluded that the beam flux is 10^4 ph/sec with statistical error ± 100 ph/sec or 1%. If more photons are counted of 106 photons in 1 second, the beam flux is $10^6 \pm 1000$ ph/sec or 0.1%. From Figure 5.5 the average flux is $3.09 \times 10^9 \pm 5.55 \times 10^4$ ph/sec, as calculated in appendix A using Equations A.1 and A.3.

Chapter Six

Conclusions

The effect of the electrons' beam parameters (beam divergence, the electron beam size and electron beam energy spread) on the flux and the energy distribution of the Compton photons of the ThomX project is studied, using analytical formulas [2] and the CAIN simulation program.

It is found that an increase of the electron beam divergence σ_e' from 80 μrad to 800 μrad resulted in X-rays spectral broadening dominated by the horizontal one. On the other hand, an increase of the electron beam energy spread σ_e from 0.1% to 1% resulted in X-rays spectral broadening dominated by vertical one.

A good agreement, within 3%, between the results of CAIN simulations, for the given detector size and its position vector, with the results of the analytical expressions at a given the angular acceptance, was obtained.

As a CdTe detector will be used in ThomX, the characteristics γ -peaks in the energy spectrum of a ^{57}Co radioactive source using the CdTe detector were obtained and occurred at 14.4, 122, 136 keV, which are in excellent agreement with the reported values [12].

For future work, the accuracy of CAIN simulations will be compared by the experimental results when the ThomX project begins operation by the end of this year (2018) and thus the results of this work will be useful in the commissioning phase of the ThomX.

Also, the feasibility of utilizing the produced hard X-rays from ThomX project by hospitals in biomedical applications is to be explored.

References

[1] C. Bruni et. al. (2009). ***"ThomX Conceptual Design Report"*** **LAL/RT**, *http://hal.in2p3.fr/in2p3-00448278*, pp. 1-136.

[2] M. Jacquet and C. Bruni (2017). ***"Analytic expressions for the angular and the spectral fluxes at Compton X-ray sources"*** **J. Synchrotron Rad**, Vol.24, pp.312-322.

[3] H. Monard (2017). "**ThomX Status**" LAL / RT, *https://indico. cern.ch/event/668097/contributions/2796071attachments/1566100/ 2468149/ARIES-workshop*_ThomX_Commissioning_HMonard.pdf.

[4] A. Variola et al. (2014). "**ThomX Technical Design Report** " LAL/RT, SLOLEIL/SOU-RA-3629, *http://hal.in2p3.fr/in2p3-0097128*, 2014.

[5] C. Bruni et al., in: Proceedings of IPAC (2011). "***ThomX: A high flux com- pact X-ray source***" **J. Synchrotron Rad, San Sebastian**, Spain, pp.49-55.

[6] E. Frank et al. (2003). "***Pulsed Tunable Monochromatic X-Ray Beams from a Compact Source: New Opportunities***" **American Journal of Roentgenology**, Vol.181, pp.1197-1202.

[7] A. Poseryaev et al. (2004). "**Electron Storage Ring For The Compact X-ray Source**" Proceedings of RuPAC XIX.

[8] M. Jacquet and P. Suortti (2014). ***"Radiation Therapy with Synchrotron Radiation:Achievements and Challenges***" **Physica Medica,** *http://www.sciencedirect.com/science/article/pii/S1120179715000447* , Vol.31, pp.596 - 600, 2014.

[9] J. Brownet al. (2001). " ***Low emittance electron beam formation with a 17GHz RF gun***" **Physical Review Special Topics - Accelerators and Beams**, Vol. 4.

[10] H. Abualrob al. (2013). "**Study the effect of a Robinson wiggler at SOLEIL towards brightness increase**”, *https://slideplayer.com/slide/4377095*.

[11] D. Sordo et al. (2009). "***Progress in the Development of CdTe and CdZnTe Semiconductor Radiation Detectors for Astrophysical and Medical Applications***" **Sensors**, Vol.9, pp.3491–3526.

[12] O. Kistner and A. Sunyar (1995). "***Excited States of*** ^{57}***Fe Populated in*** ^{57}***Co Decay***" **American Physical Society**, Vol.139, pp.B295–B299.

[13] H. Lemmer et al. (1995). "***The Decay of Cobalt -57***" **Proceedings of the Physical Society**. Section A, Vol.68, pp.701.

[14] A. Salda et al. (2012). "**High Density Devices Applied to a Gamma-Camera Implementation**" Proceedings Technique and application.

[15] J. Brian et al. (2010). "***Photon Interactions with Matter***" **Nuclear Medicine Radiation Dosimetry: Advanced Theoretical Principles**, *http://dx.doi.org/10.1007/978-1-84882-126-2_6*, p.171-207.

[16] G. Zha et al. (2012). "***The analysis of X-ray response of CdZnTe detectors***" **Science China Technological Sciences**, Vol.55, pp.2295-2299.

[17] "**Table of X-ray Emission Lines**" *http://fisica.uc.pt/data/20082009/apontamentos/apnt_339_10.pdf.*

[18] K. Yokoya et al. (2009). "**User's manual of CAIN** " *, https://ilc.kek.jp/~yokoya/CAIN/Cain242/CainMan242.pdf.*

[19] D. Sordo et al. (2017). "**CAIN modifications for PSI collisions**" Photon Beams Workshop 2017, Italy.

[20] "**Spherical Coordinate**", *https://www.quora.com/When-do-I-best-use-spherical-coordinates-and-when-cylindrical.*

[21] L. David et al. (2007). "***Error bars in experimental biology***" **The Journal of Cell Biology**, Vol.177, pp.7-11, 2007

Appendix A

Details of Flux Calculation

For calculating X-ray flux shown in Figures 4.10, 4.13 and 4.16 from the CAIN simulations, the number of macro-particle/surface and the weight of macro-particle are obtained for each simulation. In general, the X-ray flux is given by:

$$Flux = \frac{Number\ of\ photons\ (N_p)}{Periodic\ time\ (T_0)} \tag{A.1}$$

where the periodic time (T_0) and the number of X-ray photons are given by Equation A.2 and Equation A.3, respectively:

$$T_0 = \frac{Circumference}{Speed\ of\ light} \tag{A.2}$$

$$N_p = (Number\ of\ macro\ particle) \times weight \times factor \tag{A.3}$$

where the weight, which is equal to the number of X-ray photons in each group, is obtained from the CAIN simulation and equal to 49.296. The factor 10^{-2} for the input of CAIN is included in Equation A.3 because I multiplied the energy of the laser photon pulse by a factor of 10^2 (3000 mJ instead of being 30 mJ). This is done in order to improve statistics. In order to get the number of macro-particle from the obtained value of number of macro-particle/surface we use Equation A.4

$$number\ of\ macro\ particle = (Number\ of\ macro\ particle/surface) \times surface \tag{A.4}$$

where the surface is given by:

$$surface = \pi\, r^2\, [\sin^2(\theta_f) - \sin^2(\theta_i)] \tag{A.5}$$

ThomX, r =10 m and $\Delta\theta$ depends on the number of bin I used in graphs

4.10, 4.13 and 4.16 and it is equal to $\Delta\theta$=0.3 mrad. The calculated surface area is 1.413×10^{-4} m^2. The X-ray flux is then calculated by using Equation A.6.

$$Flux = \frac{(Number\ of\ macro\ particle/surface) \times surface \times weight \times factor}{Periodic\ time\ (T_0)} \tag{A.6}$$

For example, in Figure 4.13 the calculated value of the on-axis X-ray flux is 8.831×10^9 ph/sec by using the obtained value of the macro-particle/surface (from the CAIN simulation) which is equal to 7.10×10^6.

جامعة النجاح الوطنية
كلية الدراسات العليا

محاكاة ودراسة أول شعاع سيني من مشروع تومكس

إعداد
هند سليم شاهد

اشراف
أ. د. غسان سفاريني
د. أحمد بصلات

قُدمت هذه الأطروحة استكمالاً لمتطلبات الحصول على درجة الماجستير في الفيزياء في كلية الدراسات العليا في جامعة النجاح الوطنية، نابلس.

2018

محاكاة ودراسة أول شعاع سيني من مشروع تومكس

إعداد

هند سليم شاهد

إشراف

أ. د. غسان سفاريني

د. أحمد بصلات

الملخص

تقدم هذه الأطروحة دراسة على التدفق الزواني والمكاني لمصدر الأشعة السينية الناتج عن ظاهرة كومبتون العكسية مشروع تومكس، الذي يعتبر اختصاراً لظاهرة طومسون لانتاج الأشعة السينية. تنشأ هذه الأشعة السينية من خلال الارتداد المعاكس لظاهرة كوميتون بين حزمة إلكترونات ونبضه ليزر.

تم إجراء خطوتين لحساب التدفق الزاوي للأشعة السينية "كومبتون". في الخطوط الأولى، تمت كتابة برنامج محوسب قصير باستخدام صيغ تحليلية كدالة لخصائص حزمة الإلكترونات الواردة، مما سمح بحساب التدفق الزاوي والمكاني المتوقع لمصدر كومبتون. في الخطوة الثانية تم استخدام برنامج CAIN لمحاكاة توليد فوتونات كومبتون من أجل وصف التدفق والانتشار المكاني والزاوي للأشعة السينية والتحقق من التوافق بين نتائج الصيغ التحليلية ونتائج المحاكاة.

أُخذَت معاملات الكاشف CdTe (حجم الكاشف والمسافة حتى نهاية المحطة)، والذي سيستخدم في مشروع تومكس، بعين الاعتبار في المحاكاة. من المميزات الهامة أنه تم تشغيل برنامج المحاكاة على الخادم الرئيسي في مركز LAL.

بعد الحصول على أفضل معاملات للإلكترونات من نتائج الصيغ التحليلية في تومكس والتي سمحت بإنتاج أعلى تدفق كومبتون ضمن نطاق وزاوية معينين. دُرسَ تأثيرها على التدفق أشعة كومبتون باستخدام برنامج المحاكاة.

وأخيراً تم معايرة كاشف CdTe والذي سيستخدم في مشروع تومكس، باستخدام ^{57}Co كمصدر إشعاعي.